Interface focus

J. R. Soc. Interface (2009) **6**, S341–S348
doi:10.1098/rsif.2008.0425.focus
Published online 23 December 2008

REVIEW

Interconnected porous hydroxyapatite ceramics for bone tissue engineering

Hideki Yoshikawa*, Noriyuki Tamai, Tsuyoshi Murase and Akira Myoui

Department of Orthopaedic Surgery, Osaka University Graduate School of Medicine, 2-2 Yamadaoka, Suita 565-0871, Japan

Several porous calcium hydroxyapatite (HA) ceramics have been used clinically as bone substitutes, but most of them possessed few interpore connections, resulting in pathological fracture probably due to poor bone formation within the substitute. We recently developed a fully interconnected porous HA ceramic (IP-CHA) by adopting the 'foam-gel' technique. The IP-CHA had a three-dimensional structure with spherical pores of uniform size (average 150 μm, porosity 75%), which were interconnected by window-like holes (average diameter 40 μm), and also demonstrated adequate compression strength (10–12 MPa). In animal experiments, the IP-CHA showed superior osteoconduction, with the majority of pores filled with newly formed bone. The interconnected porous structure facilitates bone tissue engineering by allowing the introduction of mesenchymal cells, osteotropic agents such as bone morphogenetic protein or vasculature into the pores. Clinically, we have applied the IP-CHA to treat various bony defects in orthopaedic surgery, and radiographic examinations demonstrated that grafted IP-CHA gained radiopacity more quickly than the synthetic HA in clinical use previously. We review the accumulated data on bone tissue engineering using the novel scaffold and on clinical application in the orthopaedic field.

Keywords: bone; ceramics; hydroxyapatite; tissue engineering; mesenchymal cell

1. INTRODUCTION

When bone grafts are required for bony defects in orthopaedic surgery, autogenous bone grafting has been the gold standard because of its obvious advantages in osteogenic potential, mechanical properties and the lack of adverse immunological response. On the other hand, autogenous bone grafting has some limitations, such as the requirement of additional surgery for harvesting, the availability of sufficient grafts in size and shape and the risk of donor-site morbidity (Banwart *et al.* 1995; Arrington *et al.* 1996), which may include long-lasting pain, fracture, nerve damage and infection. Although allogeneic bone is widely used in the USA, its use is quite limited in Japan, accounting for as little as 3 per cent of procedures (Prolo & Rodrigo 1985), presumably owing to religious difficulties with using tissue from other people or corpses, as well as the lack of a well-organized tissue bank system. In addition, allograft carries the risk of transmission of occult disease, or a host immune response, which can sometimes result in complete resorption of the grafts. Therefore, many kinds of biomaterials have been developed as bone substitutes, such as hydroxyapatite (HA), alumina, zirconia, bioglass, polymers, metal, and organic or inorganic bone substitutes (Sartoris *et al.* 1986; Bucholz *et al.* 1987; Fujibayashi *et al.* 2003; Nishikawa & Ohgushi 2004).

HA ceramics have been used extensively as a substitute in bone grafts (Holmes *et al.* 1987; Bucholz *et al.* 1989), because the crystalline phase of natural bone is similar to HA. Since the 1980s, blocks and granules of porous calcium HA ceramics (CHA) have been used in orthopaedic, dental or craniofacial surgery (Uchida *et al.* 1990; Yoshikawa & Uchida 1999; Matsumine *et al.* 2004). However, there are few reports which indicate that the pores of implanted CHA are totally filled with newly formed host bone (Nakasa *et al.* 2005), probably owing to the closed structures of these CHA with few interpore connections (Ayers *et al.* 1998).

Therefore, the development of porous CHA with interpore connections of adequate diameter as well as adequate strength has long been expected as an ideal bone substitute (Roy *et al.* 2003; Simon *et al.* 2003, 2007, 2008). We recently developed a fully interconnected porous HA ceramic (IP-CHA; porosity 75%, average pore size 150 μm and average interconnections 40 μm) by adopting a 'foam-gel' technique, crosslinking polymerization that gelatinizes through the foam-like slurry in a moment (Tamai *et al.* 2002). The interconnected porous structure facilitates bone

*Author for correspondence (yhideki@ort.med.osaka-u.ac.jp).

One contribution of 10 to a Theme Supplement 'Japanese biomaterials'.

Received 11 November 2008
Accepted 28 November 2008

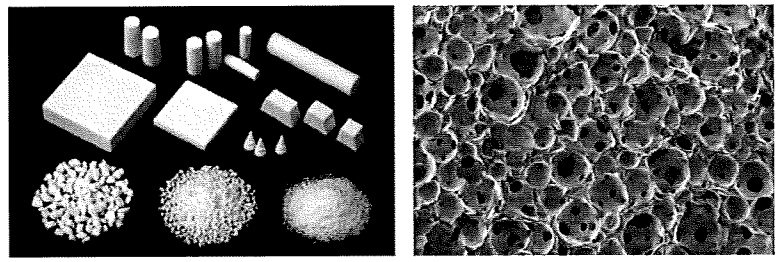

Figure 1. Interconnected porous HA ceramics (IP-CHA). (*a*) Macroscopic images of IP-CHA. The materials were manufactured by Covalent Materials Corporation. (*b*) SEM image of the microstructures of IP-CHA. Spherical pores (100–200 μm in diameter) are divided by thin walls and interconnected by interpores (10–80 μm in diameter).

tissue engineering by allowing the introduction of mesenchymal cells, osteotropic agents or vasculature into the pores. In this review, we report a new bone tissue engineering system using IP-CHA, a preliminary clinical result in patients treated with IP-CHA and a new clinical trial using a prefabricated IP-CHA in orthopaedic surgery.

2. CONVENTIONAL HYDROXYAPATITE CERAMICS IN JAPAN

The crystalline phase of natural bone is basically HA, and HA ceramics have been used extensively as a substitute in bone grafts. The ceramics are available as dense or porous types and the shape types are granular or block-like. Different pore sizes, porosities and strengths are available. Here, we describe four types of conventional HA (the first generation) that were used clinically.

— *BONEFIL* (*Mitsubishi Materials Corporation*). The types of ceramics are porous blocks and porous granules, and are most often used in orthopaedics. The sintering temperature is 900°C and the compression strength is 15 MPa/2 to 3 MPa. The pore shape is spongiose and the pore size is 200–300 μm. The degree of porosity is 60–70 per cent.

— *BONETITE* (*Mitsubishi Materials Corporation*). The types of ceramics are porous blocks and dense granules, and are most often used in dental surgery. The sintering temperature is 1200°C. The pore shape is spongiose and the pore size is 200 μm. The degree of porosity is 70 per cent.

— *BONECERAM* (*Sumitomo Osaka Cement Co. Ltd*). Porous block and porous granular types of the ceramics are available as BONECERAM-P. The sintering temperature is 1150°C. The compression strength is 44.1–68.6 MPa and the bending strength is 12.7–19.6 MPa. The pore shape is spherical and the pore size is 50–300 μm. The degree of porosity is 35–48 per cent. Dense block types of the ceramics having a high mechanical strength are available as BONECERAM-K. The sintering temperature is 1150°C. The bending strength is over 58.8 MPa.

— *APACERAM* (*PENTAX Corporation*). The types of ceramics are both dense and porous. The porous ceramic has a degree of porosity of 15–60 per cent. The sintering temperature is 1200°C. The compression and bending strengths vary from 16 to 250 MPa and 8 to 47 MPa, respectively. The better mechanical properties are associated with a decrease in the degree of porosity. The pore shape is spherical. The pore structure is an interconnected bimodal pore configuration consisting of a combination of 300 μm macropores and 2 μm micropores. The dense HA has a degree of porosity of less than 0.8 per cent. The sintering temperature is 1050°C. The compression and bending strengths are 750 and 210 MPa, respectively. Clinical applications began in 1985, with approximately 5000 clinical uses of APACERAM ceramics (custom-designed porous type plate) in cranioplasty since then. The numbers of clinical cases involving spinal surgery and ENT surgery with ear ossicle substitutes are 70 000 and 20 000, respectively.

All four of these manufactured HA ceramics are without effective interpore connections and essentially non-resorbable.

3. INTERCONNECTED POROUS HYDROXYAPATITE CERAMICS

The conventional method used to manufacture synthetic porous HA ceramics is by sintering a HA slurry mixed with organic polymer beads (Uchida *et al.* 1984). The polymer beads melt and vaporize during the sintering process, eventually leaving pores in the ceramic material. However, the pores resulting from this method are irregular in size and shape and not fully interconnected with one another. Together with Covalent Materials Corporation, MMT Co. Ltd and National Institute for Materials Science, Biomaterials Center, we developed an IP-CHA (porosity 75%, average pore size 150 μm and average interpore connections 40 μm) by adopting the foam-gel technique (figure 1; Tamai *et al.* 2002). This approach involves a crosslinking polymerization step that gelatinizes the foam-like CHA slurry in a rapid manner, thus promoting the formation of an interconnected porous structure. Briefly, the new method is as follows. (i) Slurry preparation: the slurry was prepared by mixing HA (60 wt%) with a crosslinking substrate (polyethyleneimine, 40 wt%). (ii) Foaming and gelatinization: the slurry was mixed with a foaming agent (polyoxyethylene lauryl ether, 1 wt%) and stirred until the mixture had a foamy appearance. Pore size was controlled by regulating the stirring time.

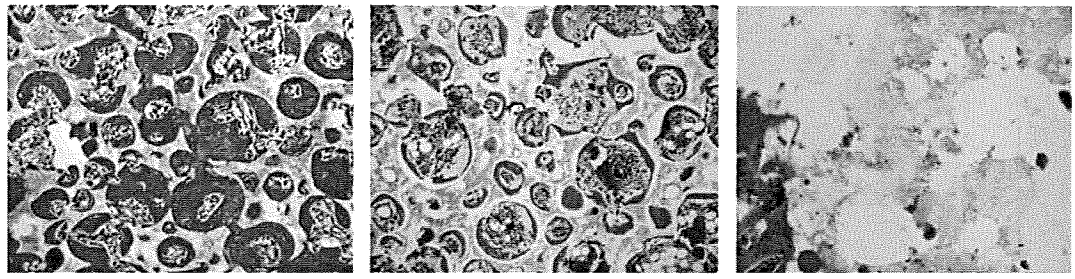

Figure 2. New bone formation within the IP-CHA in rabbit femoral condyle (HE staining×100). (*a*) Most of the pores were filled with newly formed bone at 2 weeks and (*b*) bone marrow formation was detected at 6 weeks. (*c*) In contrast, bone formation was not observed in the control group (conventional HA without interpore connections).

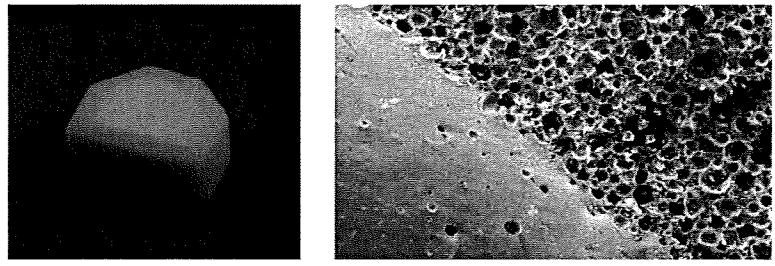

Figure 3. (*a*) Macroscopic and (*b*) microscopic (SEM) images of the solid/interconnected porous HA composite. Mechanical strength of the solid and the porous part is 550–570 and 10–12 MPa, respectively.

(iii) Gelatinization: to gelatinize the foamed slurry, another water-soluble crosslinking agent (polyfunctional epoxy compound) was added and the mixture was cast by pouring into a mould. The porous structure stabilized in less than 30 min. The foamy HA gel was removed from the mould, dried and sintered at 1200°C.

Scanning electron microscopy (SEM) analysis revealed that most of the IP-CHA pores were spherical, similar in size, approximately 100–200 μm in diameter, and showed uniform connections with one another. The wall surface of IP-CHA was very smooth and HA particles were aligned closely to one another and bound tightly.

The majority of the interpore connections ranged from 10 to 80 μm in diameter, with a maximum peak of approximately 40 μm, which would theoretically allow cell migration or tissue invasion from pore to pore (Steinkamp *et al.* 1976). Interpore connections larger than 10 μm accounted for as much as 91 per cent of the total porosity in IP-CHA. The calculated available porosity, the proportional volume of pores in the material that were connected by interpore connections larger than 10 μm in diameter, was 73.4 per cent (total porosity)×0.91=67.1 per cent. The compression strength was 12 MPa, while the compression strength of cancellous bone is 1–12 MPa (Martin *et al.* 1993).

4. OSTEOCONDUCTION *IN VIVO*

Macroporosity is known to influence the biological performance of calcium phosphate *in vivo*. Holmes *et al.* (1988) reported that pores of approximately 100 μm in diameter could provide a framework for bone growth into the pore, which then becomes vascularized easily. Most of the pores of IP-CHA are large enough to show such criteria and, more importantly, the pores are fully interconnected and more likely to allow bone ingrowth. Cylindrical blocks (6 mm in diameter) of IP-CHA were implanted into rabbit femoral condyle, and the bone ingrowth was histologically analysed (Tamai *et al.* 2002; Myoui *et al.* 2004; Yoshikawa & Myoui 2005). Within six weeks after implantation of IP-CHA, mature bone ingrowth was seen in most of the pores throughout the block. In the pores, bone, bone marrow formation through interpore connections with osteoblastic rimming and vessels were all observed (figure 2). We also examined the sequential change in the compression strength of IP-CHA implanted in rabbit femoral condyle. The initial compression strength of IP-CHA was approximately 10–12 MPa. The implanted IP-CHA steadily increased its compression strength with time until nine weeks after implantation, finally reaching a value of approximately 30 MPa (Tamai *et al.* 2002).

Recently, in order to reinforce its initial mechanical strength, we have developed a novel composite with the solid form of HA. Figure 3 shows the macroscopic and microscopic images of the solid/interconnected porous HA composite (Kaito *et al.* 2006). The mechanical strength of the solid part is 550–570 MPa, thus the solid part may correspond to cortical bone, and the porous part to cancellous bone. We constructed an implant and used a canine lumbar interbody fusion model to evaluate bone conduction of the implant and its efficacy for bony fusion. Six months after the surgery, the implant exhibited almost the same efficacy for bony fusion as iliac bone grafts. Moreover, pores of the porous part of the implant were completely filled with newly formed bone and bone marrow cells (Kaito *et al.* 2006).

5. CLINICAL APPLICATION IN ORTHOPAEDIC SURGERY

HA is a useful material to fill bone defects in treating benign bone tumours because of its biocompatibility,

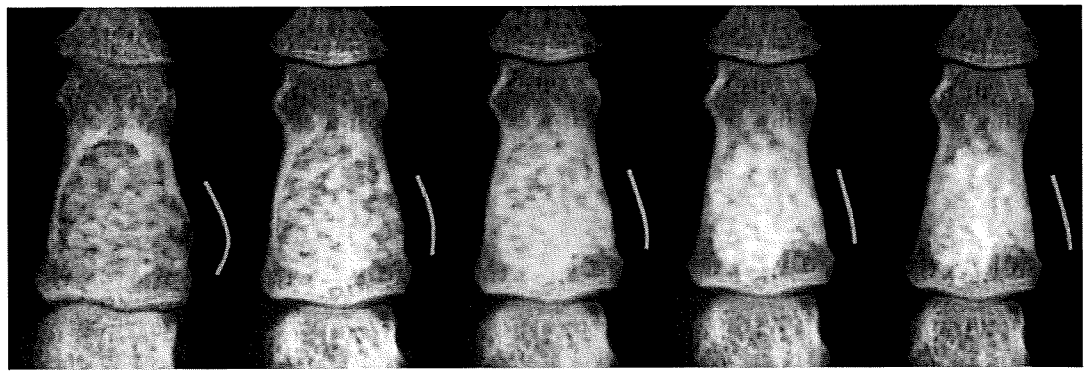

Figure 4. Clinical application of IP-CHA in the treatment of patients with bone tumours. An enchondroma of mid-phalanx, 28-year-old male. As radiodensity increased, the affected bone was remodelled, and the expansive deformity was self-corrected. (*a*) Just after surgery, (*b*) 3 months after surgery, (*c*) 6 months after surgery, (*d*) 12 months after surgery and (*e*) 27 months after surgery.

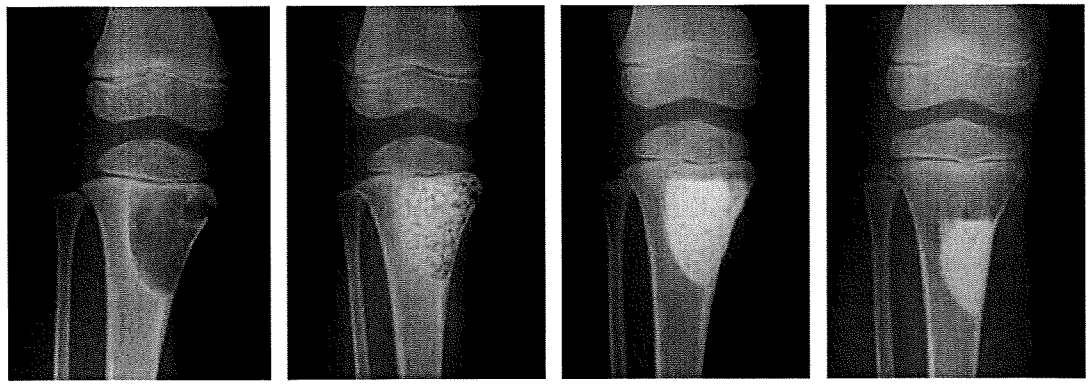

Figure 5. Clinical application of IP-CHA in the treatment of patients with bone tumours. A simple bone cyst of proximal tibia, 5-year-old boy. (*a*) Before surgery, (*b*) just after surgery, (*c*) 6 months after surgery and (*d*) 36 months after surgery.

osteoconduction and convenience, and it eliminates the need for additional surgery for harvesting autograft, as we reported previously (Uchida *et al.* 1990; Yoshikawa & Uchida 1999; Matsumine *et al.* 2004). However, as a late complication, pathological fractures of the implanted sites have been reported (Yoshikawa & Uchida 1999; Matsumine *et al.* 2004). This is probably due to poor bone ingrowth in the material as a result of poor incorporation of the material into the host bone. We applied IP-CHA as a bone substitute for the treatment of 59 patients with benign bone tumours at the Osaka University Hospital and its affiliated hospitals. The average age of patients was 32 years (range 5–75 years). The tumours were located in the upper extremities in 25 patients, lower extremities in 27 and pelvis in 7. The mean follow-up period was 46 months (range 32–60 months). After adequate removal of the tumours, IP-CHA blocks and/or granules of 2–5 mm in diameter were used to fill the bony defects. We also used IP-CHA to fill 12 cystic lesions with rheumatoid arthritis (Shi *et al.* 2006). None of the patients showed any signs of inflammatory reaction, rejection, infection or abnormal results in blood tests. Neither pathological fracture nor deformity was observed at the implanted site based on radiographic examinations during the follow-up period. The radiographic examinations were periodically carried out and revealed that the radiolucent line between the implanted IP-CHA and host bone tended to decrease with time after surgery and eventually disappeared (figure 4). The radiographic density at the implanted site increased with time and the IP-CHA granules appeared to fuse with one another, eventually forming a dense radiopaque shadow. Interestingly, longitudinal bone growth was not disturbed even when IP-CHA was implanted in close proximity to the growth plate of children (figure 5). Gadolinium-enhanced MRI showed a ring enhancement at the periphery of the implant (data not shown) and the area with enhancement advanced towards the centre of the implant, indicating that bone regeneration with blood supply might occur within the IP-CHA.

The IP-CHA can be prefabricated into specific sizes and shapes to match bone defects. We did this to make an implant, which was, in advance, planned and reconstructed with a computer-aided design/manufacturing (CAD/CAM) system. A three-dimensional image was reconstructed with the CT data of the estimated bony defect, and the IP-CHA was fabricated by a three-dimensional milling machine (Roland DG, MDX-20; figure 6). We have used the prefabricated IP-CHA for various bony defects in orthopaedic surgery, and obtained a satisfactory clinical outcome.

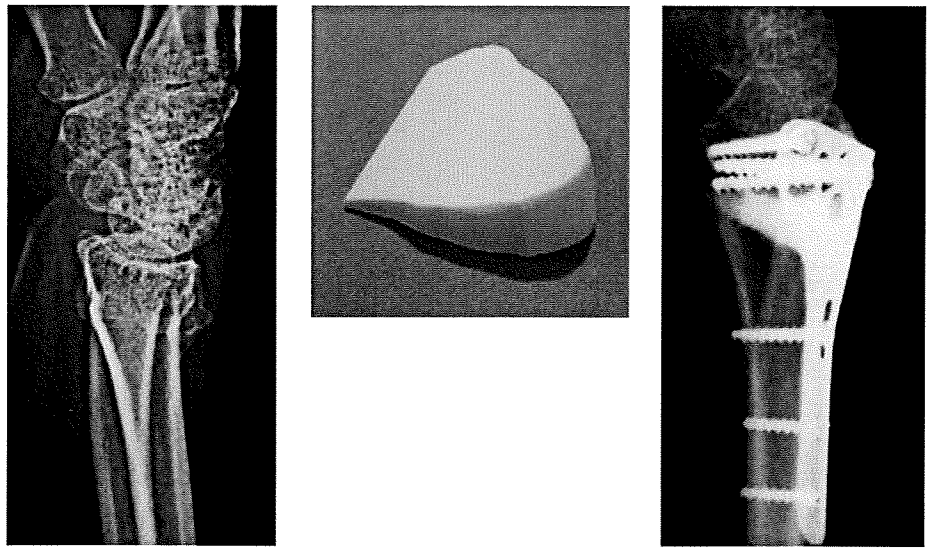

Figure 6. Correction osteotomy for malunited fracture of the distal radius, 48-year-old woman. (*a*) Preoperative X-ray image of the affected radius, six months after the fracture of the distal radius. (*b*) Prefabricated IP-CHA. A three-dimensional image was reconstructed with the CT data of the estimated bony defect after correction, and the IP-CHA was fabricated by a three-dimensional milling machine (Roland DG, MDX-20). (*c*) Post-operative X-ray image, a year after surgery. The malalignment was satisfactorily corrected by the surgery using the prefabricated IP-CHA and a metal plate.

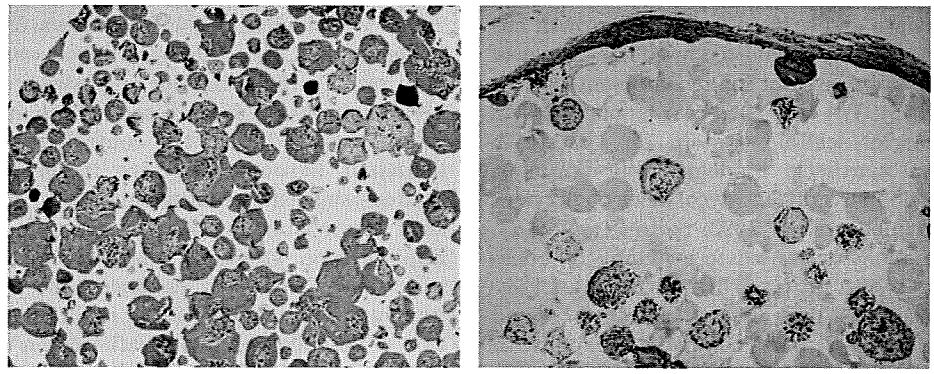

Figure 7. Bone tissue engineering by mesenchymal stem cells (HE staining×40). (*a*) At eight weeks after implantation, extensive bone volume was detected not only in the surface pore areas but also in the centre pore areas of IP-CHA. (*b*) In the control group (conventional HA without interpore connections), little bone formation was observed even in the surface pore areas.

6. BONE TISSUE ENGINEERING BY MESENCHYMAL STEM CELLS

The IP-CHA can be used as a scaffold for cell-based bone tissue engineering. We tested the efficacy of IP-CHA using a rat subcutaneous model by Ohgushi & Caplan (1999). Bone marrow cells were collected from the femur of rat and were cultivated in minimal essential medium supplemented with 15 per cent foetal bovine serum. IP-CHA discs (R=5 mm, h=2 mm) were soaked in the cell suspension overnight and further cultured in the same medium with β-glycerophosphate, ascorbic acid and dexamethasone for 14 days. The discs were then implanted into the subcutaneous tissue of rats and harvested for two to eight weeks after implantation. All the implants showed bone formation inside the pore areas as evidenced by decalcified histological sections and microcomputed tomography images (Nishikawa *et al.* 2004, 2005). At eight weeks after implantation, extensive bone volume was detected not only in the surface pore areas, but also in the centre pore areas of the implants (figure 7). The combination of IP-CHA and mesenchymal cells could be used as an excellent bone graft substitute because of its mechanical properties and capability of bone formation.

Recently, we have started a clinical trial with the combination of IP-CHA and autologous mesenchymal cells for bone tissue repair, and already treated 10 patients.

A precise clinical evaluation is necessary, but we believe that bone tissue engineering by IP-CHA offers new approaches to treatment for patients requiring skeletal reconstruction.

7. BONE TISSUE ENGINEERING BY BONE MORPHOGENETIC PROTEIN

Bone morphogenetic proteins (BMPs) are biologically active molecules capable of inducing new bone formation, and show potential for clinical use in bone defect repair

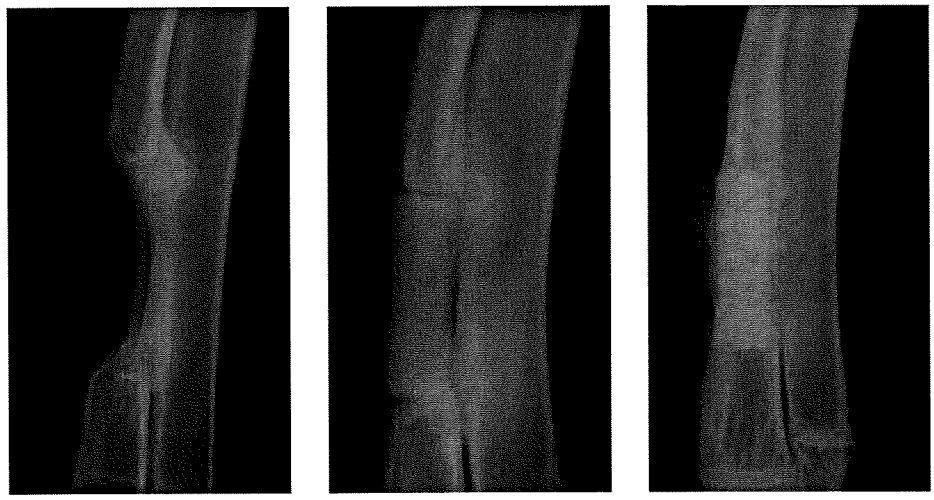

Figure 8. Bone healing by IP-CHA combined with BMP. (*a*) No implant group at eight weeks after surgery. No bone formation was detected. (*b*) IP-CHA group alone at eight weeks after implantation. Radiolucent lines were clearly visible between IP-CHA and host bone. (*c*) rhBMP-2 (5 μg)/IP-CHA group at eight weeks after implantation. Bony unions were observed at the junction sites and the radiodensity of IP-CHA increased.

(Wozney & Rosen 1998; Nakase & Yoshikawa 2006). However, an ideal system for delivering BMPs that can potentiate their bone-inducing ability and provide initial mechanical strength and scaffold for bone ingrowth has not yet been developed. We have analysed the efficacy of IP-CHA as a delivery system for recombinant human BMP-2 (rhBMP-2). We combined two biomaterials to construct a carrier/scaffold system for rhBMP-2: IP-CHA and a synthetic biodegradable polymer, poly-D,L-lactic acid–polyethyleneglycol block co-polymer (PLA-PEG; Miyamoto *et al.* 1993; Saito *et al.* 2001). A rabbit radius model was used to evaluate the bone-regenerating activity of the rhBMP-2/PLA-PEG/IP-CHA composite. All bone defects in groups treated with 5 μg of rhBMP-2 were completely fixed with sufficient strength at eight weeks after implantation (Kaito *et al.* 2005; figure 8). Using this carrier scaffold system, we reduced the amount of rhBMP-2 necessary for such results to approximately one-tenth of the amount needed in previous studies. Enhancement of bone formation is probably due to the superior osteoconduction ability of IP-CHA and the optimal drug delivery system provided by PLA-PEG. The PLA-PEG/IP-CHA composite is an excellent carrier/scaffold delivery system for rhBMP-2, and strongly encourages the clinical effects of rhBMP-2 in bone tissue regeneration.

8. BONE TISSUE ENGINEERING BY VASCULAR PREFABRICATION

Vascular network invasion into porous implants is another important aspect of using such materials as bone substitutes for large bone defects or in the construction of tissue-engineered bone, because cells cannot survive farther than a few hundred micrometres from a nutrient supply. The rate of new bone ingrowth into the porous material depends on vascular invasion from the surface of the implant, which is not fast enough in large implants to transport nutrients to cells transplanted in pores of the implant. Therefore, we examined whether prefabrication of IP-CHA with a vascular bundle enhances vascular network invasion into the pores via interpore connections (Akita *et al.* 2004; Myoui *et al.* 2004; Yoshikawa & Myoui 2005). When an IP-CHA cylindrical block was prefabricated with rat superficial inferior epigastric vessels, vascular invasion in the pores increased in both number and size, when compared with the control, resulting in more abundant fibrous connective tissue formation. Our findings suggest that inserting a vascular bundle into such interconnecting porous implants at the site of implantation supports vascular network invasion, which may eventually enhance bone ingrowth in the implants. Nakasa *et al.* (2005) reported that prefabrication of vascularized bone graft using a combination of fibroblast growth factor-2 and vascular bundle implantation into IP-CHA led to a satisfactory result in the reconstruction of bony defects.

9. APPLICATION FOR CARTILAGE REPAIR AND TENDON ATTACHMENT

We have developed a new technology for articular cartilage repair, consisting of a triple composite of rhBMP-2, PLA-PEG and IP-CHA, to induce the regeneration of both subchondral bone and articular cartilage (Tamai *et al.* 2005). Full-thickness cartilage defects in the rabbit were filled with the rhBMP-2 (20 μg)/PLA-PEG/IP-CHA composite. At six weeks, subchondral defects were completely repaired by subchondral bone and articular cartilage covering the bone. The regenerated cartilage manifested a hyaline-like appearance, with a columnar organization of chondrocytes and a mature matrix. The novel cell-free technology, the triple composite of rhBMP-2, PLA-PEG and IP-CHA, could mark a new development in the field of articular cartilage repair. Our new strategy for articular cartilage repair seems to be unique for the following three reasons: (i) we used autogenous mesenchymal cells efficiently recruited from bone

marrow by strongly activating the regeneration process of the subchondral bone defect, (ii) continuous BMP stimuli seemed to promote both the vigorous regeneration of subchondral bone and the following chondrocytic differentiation and cartilaginous matrix production at the surface resulting in hyaline-like cartilage regeneration in as little as three weeks, and (iii) the regenerated cartilage exhibited almost perfect lateral integration with the surrounding host cartilage, probably because the whole regeneration process in this system was *in situ* and efficient, unlike an *ex vivo* chondrocyte culture system. Ito *et al.* (2008) reported that an osteochondral plug using cultured chondrocytes and cylindrical IP-CHA plugs was successful in treating osteochondral defects in a rabbit model. Ohmae *et al.* have also tried to enhance tendon attachment to bone using IP-CHA with bone marrow stromal cells in a rabbit model, and obtained a satisfactory result (Omae *et al.* 2006, 2007).

10. CONCLUSIONS

The foam-gel technique is an innovative method that generates a three-dimensional fully interconnected porous structure in synthetic HA ceramics. The interconnected porous structure encourages bone ingrowth into the material and eventually leads to good incorporation of the material into the host bone. Our study indicated that IP-CHA exhibited excellent bone ingrowth in an animal model and favourable performance in clinical use. We believe that IP-CHA is an excellent bone substitute for filling bone defects and should be considered as an alternative to autogenous bone. In addition, IP-CHA seems likely to serve as a good scaffold for cell-based or cytokine-based tissue-engineered bone. In fact, we have been successful in bone tissue engineering using rhBMP-2, mesenchymal cells or vasculature in animals. The synthetic scaffold can be prefabricated into specific sizes and shapes to match bone defects, and even into a composite with the solid form of HA in order to reinforce its initial mechanical strength. IP-CHA is now commercially available in Japan, and we have applied IP-CHA as a bone substitute for the treatment of more than 80 patients with benign bone tumours or rheumatoid arthritis, and obtained some favourable clinical results. Recently, we have started a clinical trial with the combination of IP-CHA and autologous mesenchymal cells for bone tissue repair. Additional studies with larger animals including dogs or monkeys and precise clinical evaluation are necessary, but we believe that bone tissue engineering by IP-CHA offers new approaches to the treatment of patients requiring skeletal reconstruction.

The authors would like to thank Dr Kunio Takaoka for his invaluable advice regarding bone tissue engineering using rhBMP-2, and Dr Hajime Ohgushi for his invaluable advice regarding bone tissue engineering using bone marrow cells. We also thank Covalent Materials Corporation and MMT Co. Ltd for supplying materials. This work was supported in part by grants from the New Energy and Industrial Technology Development Organization (NEDO), the Ministry of Health, Labor and Welfare, Japan, and the Ministry of Education, Culture, Sports, Science and Technology, Japan.

REFERENCES

Akita, S., Tamai, N., Myoui, A., Nishikawa, M., Kaito, T., Takaoka, K. & Yoshikawa, H. 2004 Capillary vessel network integration by inserting a vascular pedicle enhances bone formation in tissue-engineered bone using interconnected porous hydroxyapatite ceramics. *Tissue Eng.* **10**, 789–795. (doi:10.1089/1076327041348338)

Arrington, E. D., Smith, W. J., Chambers, H. G., Bucknell, A. L. & Davino, N. A. 1996 Complications of iliac crest bone graft harvesting. *Clin. Orthop.* **329**, 300–309. (doi:10.1097/00003086-199608000-00037)

Ayers, R. A., Simske, S. J., Nunes, C. R. & Wolford, L. M. 1998 Long-term bone ingrowth and residual micro hardness of porous block hydroxyapatite implants in humans. *J. Oral Maxillofac. Surg.* **56**, 1297–1301. (doi:10.1016/S0278-2391(98)90613-9)

Banwart, J. C., Asher, M. A. & Hassanein, R. S. 1995 Iliac crest bone graft harvest donor site morbidity. A statistical evaluation. *Spine* **20**, 1055–1060. (doi:10.1097/00007632-199505000-00012)

Bucholz, R. W., Carlton, A. & Holmes, R. E. 1987 Hydroxyapatite and tricalcium phosphate bone graft substitute. *Orthop. Clin. North Am.* **18**, 323–334.

Bucholz, R. W., Carlton, A. & Holmes, R. 1989 Interporous hydroxyapatite as a bone graft substitute in tibial plateau fractures. *Clin. Orthop.* **240**, 53–62.

Fujibayashi, S., Kim, H. M., Neo, M., Uchida, M., Kokubo, T. & Nakamura, T. 2003 Repair of segmental long bone defect in rabbit femur using bioactive titanium cylindrical mesh cage. *Biomaterials* **24**, 3445–3451. (doi:10.1016/S0142-9612(03)00221-7)

Holmes, R. E., Bucholz, R. W. & Mooney, V. 1987 Porous hydroxyapatite as a bone graft substitute in diaphyseal defects: a histometric study. *J. Orthop. Res.* **5**, 114–121. (doi:10.1002/jor.1100050114)

Holmes, R. E., Wardrop, R. W. & Wolford, L. M. 1988 Hydroxylapatite as a bone graft substitute in orthognathic surgery: histologic and histometric findings. *J. Oral Maxillofac. Surg.* **46**, 661–671. (doi:10.1016/0278-2391(88)90109-7)

Ito, Y., Adachi, N., Nakamae, A., Yanada, S. & Ochi, M. 2008 Transplantation of tissue-engineered osteochondral plug using cultured chondrocytes and interconnected porous calcium hydroxyapatite ceramic cylindrical plugs to treat osteochondral defects in a rabbit model. *Artif. Organs* **32**, 36–44.

Kaito, T., Myoui, A., Takaoka, K., Saito, N., Nishikawa, M., Tamai, N., Ohgushi, H. & Yoshikawa, H. 2005 Potentiation of the activity of bone morphogenetic protein-2 in bone regeneration by a PLA-PEG/hydroxyapatite composite. *Biomaterials* **26**, 73–79. (doi:10.1016/j.biomaterials.2004.02.010)

Kaito, T., Mukai, Y., Nishikawa, M., Ando, W., Yoshikawa, H. & Myoui, A. 2006 Dual hydroxyapatite composite with porous and solid parts: experimental study using canine lumbar interbody fusion model. *J. Biomed. Mater. Res. B* **78**, 378–384. (doi:10.1002/jbm.b.30498)

Martin, R. B., Chapman, M. W., Sharkey, N. A., Zissimos, S. L., Bay, B. & Shors, E. C. 1993 Bone ingrowth and mechanical properties of coralline hydroxyapatite 1 yr after implantation. *Biomaterials* **14**, 341–348. (doi:10.1016/0142-9612(93)90052-4)

Matsumine, A., Myoui, A., Kusuzaki, K., Araki, N., Seto, M., Yoshikawa, H. & Uchida, A. 2004 Calcium hydroxyapatite

ceramic implants in bone tumor surgery. A long-term follow-up study. *J. Bone Joint Surg. Br.* **86**, 719–725. (doi:10.1302/0301-620X.86B5.14242)

Miyamoto, S., Takaoka, K., Okada, T., Yoshikawa, H., Hashimoto, J., Suzuki, S. & Ono, K. 1993 Polylactic acid-polyethylene glycol block copolymer: a new biodegradable synthetic carrier for bone morphogenetic protein. *Clin. Orthop.* **294**, 333–343.

Myoui, A., Tamai, N., Nishikawa, M., Araki, N., Nakase, T., Akita, S. & Yoshikawa, H. 2004 Three-dimensionally engineered hydroxyapatite ceramics with interconnected pores as a bone substitute and tissue engineering scaffold. In *Biomaterials in orthopedics* (eds M. J. Yaszemski, D. J. Trantolo, K. U. Lewandrowski, V. Hasirci, D. E. Altobelli & D. L. Wise), pp. 287–300. New York, NY: Marcel Dekker.

Nakasa, T., Ishida, O., Sunagawa, T., Nakamae, A., Yasunaga, Y., Agung, M. & Ochi, M. 2005 Prefabrication of vascularized bone graft using a combination of fibroblast growth factor-2 and vascular bundle implantation into a novel interconnected porous calcium hydroxyapatite ceramic. *J. Biomed. Mater. Res.* **75A**, 350–355. (doi:10.1002/jbm.a.30435)

Nakase, T. & Yoshikawa, H. 2006 Potential roles of bone morphogenetic proteins (BMPs) in skeletal repair and regeneration. *J. Bone Mineral Metab.* **24**, 425–433. (doi:10.1007/s00774-006-0718-8)

Nishikawa, M. & Ohgushi, H. 2004 Calcium phosphate ceramics in Japan. In *Biomaterials in orthopedics* (eds M. J. Yaszemski, D. J. Trantolo, K. U. Lewandrowski, V. Hasirci, D. E. Altobelli & D. L. Wise), pp. 425–436. New York, NY: Marcel Dekker.

Nishikawa, M., Myoui, A., Ohgushi, H., Ikeuchi, M., Tamai, N. & Yoshikawa, H. 2004 Bone tissue engineering using novel interconnected porous hydroxyapatite ceramics combined with marrow mesenchymal cells: quantitative and three-dimensional image analysis. *Cell Transplant.* **13**, 367–376. (doi:10.3727/000000004783983819)

Nishikawa, M., Ohgushi, H., Tamai, N., Osuga, K., Uemura, M., Yoshikawa, H. & Myoui, A. 2005 The effect of simulated microgravity by three-dimensional clinostat on bone tissue engineering. *Cell Transplant.* **14**, 829–835. (doi:10.3727/000000005783982477)

Ohgushi, H. & Caplan, A. I. 1999 Stem cell technology and bioceramics: from cell to gene engineering. *J. Biomed. Mater. Res.* **48A**, 913–927. (doi:10.1002/(SICI)1097-4636(1999)48:6<913::AID-JBM22>3.0.CO;2-0)

Omae, H., Mochizuki, Y., Yokoya, S., Adachi, N. & Ochi, M. 2006 Effects of interconnecting porous structure of hydroxyapatite ceramics on interface between grafted tendon and ceramics. *J. Biomed. Mater. Res. A* **79**, 329–337. (doi:10.1002/jbm.a.30797)

Omae, H., Mochizuki, Y., Yokoya, S., Adachi, N. & Ochi, M. 2007 Augmentation of tendon attachment to porous ceramics by bone marrow stromal cells in a rabbit model. *Int. Orthop.* **31**, 353–358. (doi:10.1007/s00264-006-0194-8)

Prolo, D. J. & Rodrigo, J. J. 1985 Contemporary bone graft physiology and surgery. *Clin. Orthop.* **200**, 322–342. (doi:10.1097/00003086-198511000-00036)

Roy, T. D., Simon, J. L., Ricci, J. L., Rekow, E. D., Thompson, V. P. & Parsons, J. R. 2003 Performance of degradable composite bone repair products made via three-dimensional fabrication techniques. *J. Biomed. Mater. Res. A* **66**, 283–291. (doi:10.1002/jbm.a.10582)

Saito, N., Okada, T., Horiuchi, H., Murakami, N., Takahashi, J., Nawata, M., Ota, H., Miyamoto, S., Nozaki, K. & Takaoka, K. 2001 Biodegradable poly-D,L-lactic acid-polyethylene glycol block copolymers as a BMP delivery system for inducing bone. *J. Bone Joint Surg.* **83A**, S92–S98.

Sartoris, D. J., Gershuni, D. H., Akeson, W. H., Holmes, R. E. & Resnick, D. 1986 Coralline hydroxyapatite bone graft substitutes: preliminary report of radiographic evaluation. *Radiology* **159**, 133–137.

Shi, K., Hayashida, K., Hashimoto, J., Sugamoto, K., Kawai, H. & Yoshikawa, H. 2006 Hydroxyapatite augmentation for bone atrophy in total ankle replacement in rheumatoid arthritis. *J. Foot Ankle Surg.* **45**, 316–321. (doi:10.1053/j.jfas.2006.06.001)

Simon, J. L., Roy, T. D., Parsons, J. R., Rekow, E. D., Thompson, V. P., Kemnitzer, J. & Ricci, J. L. 2003 Engineered cellular response to scaffold architecture in a rabbit trephine defect. *J. Biomed. Mater. Res. A* **66**, 275–282. (doi:10.1002/jbm.a.10569)

Simon, J. L., Michna, S., Lewis, J. A., Rekow, E. D., Thompson, V. P., Smay, J. E., Yampolsky, A., Parsons, J. R. & Ricci, J. L. 2007 *In vivo* bone response to 3D periodic hydroxyapatite scaffolds assembled by direct ink writing. *J. Biomed. Mater. Res. A* **83**, 747–758. (doi:10.1002/jbm.a.31329)

Simon, J. L., Rekow, E. D., Thompson, V. P., Beam, H., Ricci, J. L. & Parsons, J. R. 2008 MicroCT analysis of hydroxyapatite bone repair scaffolds created via three-dimensional printing for evaluating the effects of scaffold architecture on bone ingrowth. *J. Biomed. Mater. Res. A* **85**, 371–377.

Steinkamp, J. A., Hansen, K. M. & Crissman, H. A. 1976 Flow microfluorometric and light-scatter measurement of nuclear and cytoplasmic size in mammalian cells. *J. Histochem. Cytochem.* **24**, 292–297.

Tamai, N., Myoui, A., Tomita, T., Nakase, T., Tanaka, J., Ochi, T. & Yoshikawa, H. 2002 Novel hydroxyapatite ceramics with an interconnective porous structure exhibit superior osteoconduction *in vivo*. *J. Biomed. Mater. Res.* **59A**, 110–117. (doi:10.1002/jbm.1222)

Tamai, N., Myoui, A., Hirao, M., Kaito, T., Ochi, T., Tanaka, J., Takaoka, K. & Yoshikawa, H. 2005 A new biotechnology for articular cartilage repair: subchondral implantation of a composite of interconnected porous hydroxyapatite, synthetic polymer (PLA/PEG), and bone morphogenetic protein-2 (rhBMP-2). *Osteoarthr. Cartil.* **13**, 405–417. (doi:10.1016/j.joca.2004.12.014)

Uchida, A., Nade, S. M., McCartney, E. R. & Ching, W. 1984 The use of ceramics for bone replacement. A comparative study of three different porous ceramics. *J. Bone Joint Surg. Br.* **66**, 269–275.

Uchida, A., Araki, N., Shinto, Y., Yoshikawa, H., Kurisaki, E. & Ono, K. 1990 The use of calcium hydroxyapatite ceramic in bone tumour surgery. *J. Bone Joint Surg. Br.* **72**, 298–302.

Wozney, J. M. & Rosen, V. 1998 Bone morphogenetic protein and bone morphogenetic protein gene family in bone formation and repair. *Clin. Orthop.* **346**, 26–37. (doi:10.1097/00003086-199801000-00006)

Yoshikawa, H. & Myoui, A. 2005 Bone tissue engineering with porous hydroxyapatite ceramics. *J. Artif. Organs* **8**, 131–136. (doi:10.1007/s10047-005-0292-1)

Yoshikawa, H. & Uchida, A. 1999 Clinical application of calcium hydroxyapatite ceramic in bone tumor surgery. In *Biomaterials and bioengineering handbook* (ed. D. L. Wise), pp. 433–455. New York, NY: Marcel Dekker.

Arch Orthop Trauma Surg (2009) 129:1465–1471
DOI 10.1007/s00402-008-0800-x

ORTHOPAEDIC SURGERY

Correction of severe wrist deformity following physeal arrest of the distal radius with the aid of a three-dimensional computer simulation

Tsuyoshi Murase · Kunihiro Oka · Hisao Moritomo · Akira Goto · Kazuomi Sugamoto · Hideki Yoshikawa

Received: 12 July 2008 / Published online: 19 December 2008

Abstract Growth arrest following physeal injury may result in severe limb deformity. We report a case of complex wrist deformity caused by injury to the distal radial physis resulting in radial shortening and abnormal inclination of the radial articular surface, which was successfully treated by gradual correction after computer simulation. The simulation enabled us to develop an appropriate operative plan by accurately calculating the axis of the three-dimensional (3D) deformity using computer bone models. In the simulative surgery with a full-size stereolithography bone model, an Ilizarov external fixator was applied to the radius such that its two hinges were located on the virtual axis of the deformity, which was reproduced in the actual surgery. This technique of 3D computer simulation is a useful alternative to plan accurate correction of complex limb deformities following growth arrest.

Keywords Computer simulation · Deformity correction · Gradual lengthening · Physeal arrest · Distal radius

Electronic supplementary material The online version of this article (doi:10.1007/s00402-008-0800-x) contains supplementary material, which is available to authorized users.

T. Murase (✉) · K. Oka · H. Moritomo · A. Goto · H. Yoshikawa
Department of Orthopaedic Surgery,
Osaka University Graduate School of Medicine,
2-2, Yamada-Oka, Suita, Osaka 565-0871, Japan
e-mail: tmurase-osk@umin.ac.jp

K. Sugamoto
Department of Orthopaedic Biomaterial Science,
Osaka University Graduate School of Medicine,
2-2, Yamada-Oka, Suita, Osaka 565-0871, Japan

Introduction

Growth arrest following physeal injury to the distal radius may result in complex wrist deformities such as radial shortening and abnormal inclination of the radial articular surface, and it has been a challenging therapeutic problem [4, 14, 28, 30]. Although several previous reports have recommended gradual correction by lengthening using an external fixator, it is not always easy to devise an appropriate preoperative plan for three-dimensionally complex periarticular deformities [2, 21]. On the other hand, recent advances in computed tomography (CT) and three-dimensional (3D) image processing technology have enabled us to precisely simulate 3D correction of such difficult deformities [3, 10]. We have suggested that, in 3D computer simulation, a screw displacement axis (SDA) of the deformed segment relative to the rest of the bone appropriately serves as a 3D deformity axis, enabling the deformity correction to be planned accordingly [11, 20, 27].

We report a case of severe wrist deformity following physeal arrest of the distal radius that was successfully treated by application of an Ilizarov external fixator using a unique preoperative simulation based on the 3D deformity axis, which was calculated using an original computer program [19].

Case presentation

A 7-year-old boy sustained a fracture of the left distal radius, and was treated conservatively with a cast, although the distal fragment was displaced and malunited. Two months after the initial injury, he underwent corrective osteotomy at the same hospital; however, wrist deformity gradually developed during the follow-up period. He was

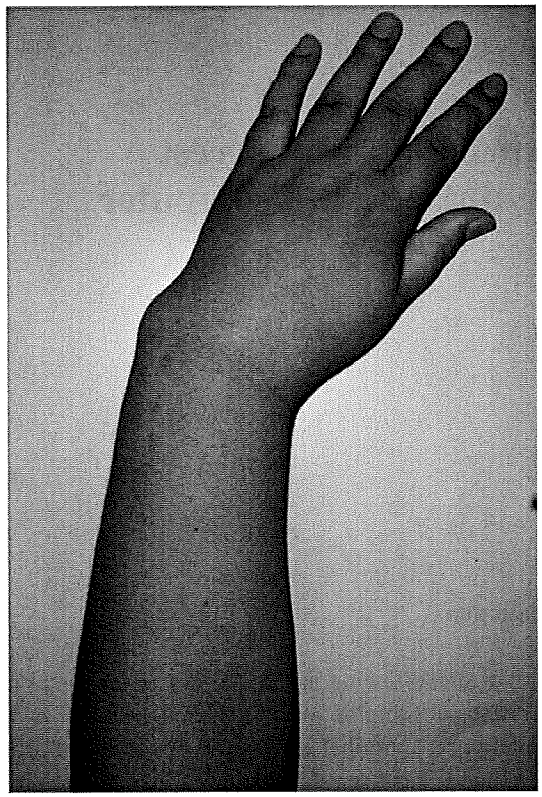

Fig. 1 Radial deviation of the wrist was obvious, and the ulnar head projected

referred to our hospital at 12 years of age when he complained of the unsightly appearance of his wrist and restricted range of wrist motion.

At first presentation, radial deviation of the wrist, and prominence of the ulnar head were obvious (Fig. 1). The range of wrist flexion was restricted to 20°, although wrist extension and forearm rotation were not impaired. Radiographs showed significant deformity of the distal radius and considerable radial and dorsal tilt with shortening (Fig. 2). MRI revealed that >50% of the physis was closed.

In order to plan corrective surgery for this complex deformity of the distal radius, we attempted to simulate 3D correction of the deformity using a computer model of the bone. First, the entire forearm was scanned by CT (GE LightSpeed Ultra16; scan time 0.5 s, slice thickness 1.25 mm, 30 mA, 120 kV), and the digital data were transferred to a computer. The contours of the radius, and ulna were semi-automatically segmented using commercially available software (Virtual Place M®, Medical Imaging Laboratory, Tokyo, Japan) and surface models of the bones were constructed by applying a 3D surface generation of the bone's cortex using Marching Cubes algorithm [15]. The geometrical models of the forearm bones were then visualized using a VTK-based original computer program (Visualization TookKit; Kitware Inc., Clifton Park, NY).

The degree of deformity of the radius can be expressed in terms of the displacement of the distal radius compared with the proximal part. The displacement is usually described by six parameters that measure rotation around and translation along the x, y, and z axes in any coordinate system; however, it can also be simply expressed as rotation around and translation along a unique axis in a SDA system (Fig. 3) [11, 27]. In this case, the axis around which the distal radius moves into normal position was calculated using the computer program. Normal position was determined using the mirror image of the contralateral normal radius as a reference. Simulation results demonstrated that the radial shortening, and abnormal articular inclination could be corrected by simply rotating the distal part of the radius by 40° around the axis that runs 3 cm volar to the wrist joint and at an angle of 60° to the transverse line of the radius (Fig. 4; see also the Supplementary video).

To investigate the feasibility of computer planning, we performed a simulative surgery with a full-size stereolithography bone model (CMET Inc., Yokohama, Japan) that was constructed from the CT data. An Ilizarov external fixator consisting of two rings at an angle of 40° to each other was attached to the radius of the resin model. The distal ring was fixed to the distal part of the radius-model with Kirschner wires, and the proximal ring was fixed to the radial diaphysis. The rings were connected by three rods. Two hinges were set on the two open-sided rods and were located on the simulated axis (Fig. 5a). By lengthening only the closed-sided rod after radial osteotomy, the distal ring together with the distal segment of the radius rotated around the simulated axis. When the two rings became parallel with each other, the distal radius rotated by 40°, resulting in simultaneous correction of the radial shortening, and dorsoradial inclination of the articular surface (Fig. 5b, c).

The stereolithography model was sterilized and brought into the operating theater as a surgical guide (Fig. 6), and the actual operation was performed according to the simulation so that the two hinges were located on the simulated axis. Lengthening began 1 week after the operation and ended after 10 weeks. Gradual correction of the radius occurred uneventfully, and new callus was well formed at the osteotomy site (Fig. 7). The external fixator was removed 15 weeks postoperatively, when adequate maturation of the callus had been confirmed through plain radiographs. A plastic orthosis was applied for another week, and then an active range of motion exercise was initiated. The radial inclination, and volar tilt on radiographs were corrected, as expected from the preoperative simulation (Fig. 8), and the appearance markedly improved after surgery (Fig. 9). The postoperative wrist flexion/extension, and forearm pronation/supination ranges of motion were 60°/80° and 80°/80°, respectively. The distal radio-ulnar joint was stable and painless.

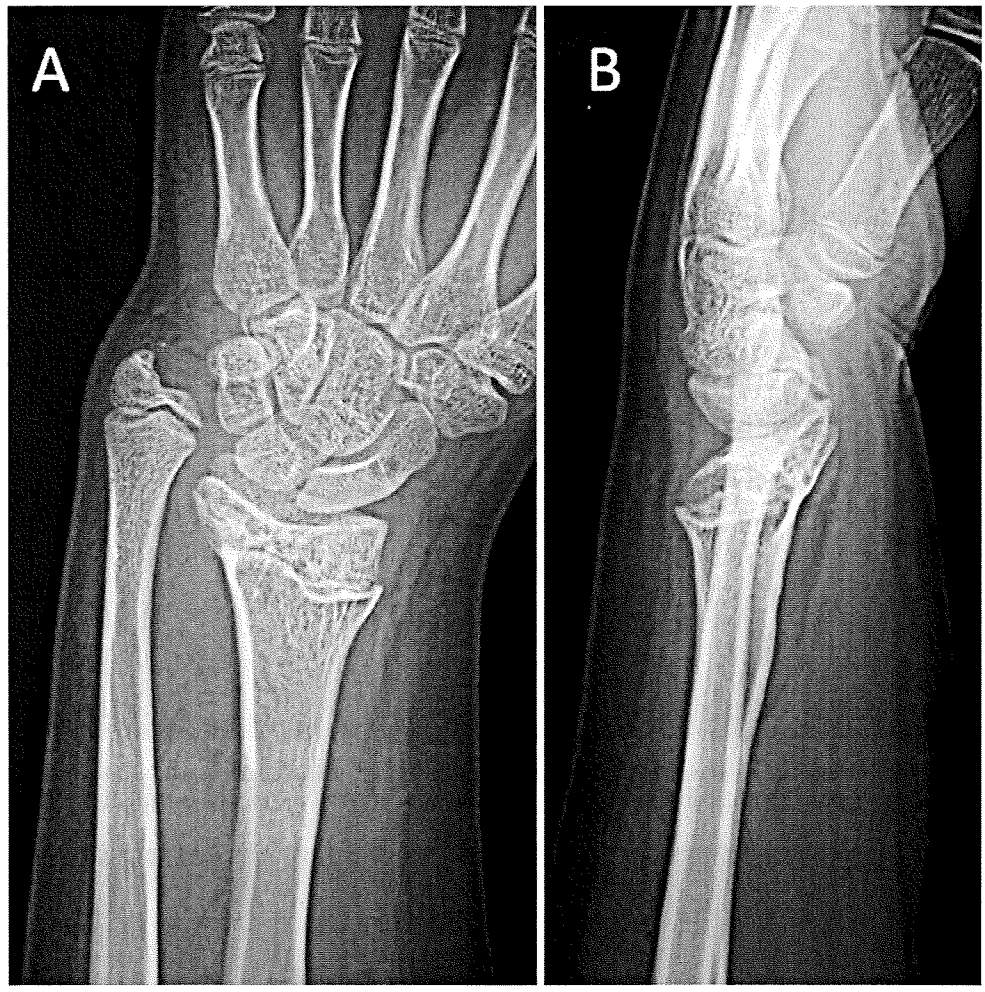

Fig. 2 **a** AP and **b** lateral radiographs showed shortening of the radius with marked radial and dorsal inclination of the articular surface

Twenty months after the operation, when the patient was 14 years of age, the ulnar variance had increased to 2 mm, but the configuration of the radial articular surface remained the same. The patient was satisfied with the appearance of the wrist and does not complain of any functional limitation in daily life.

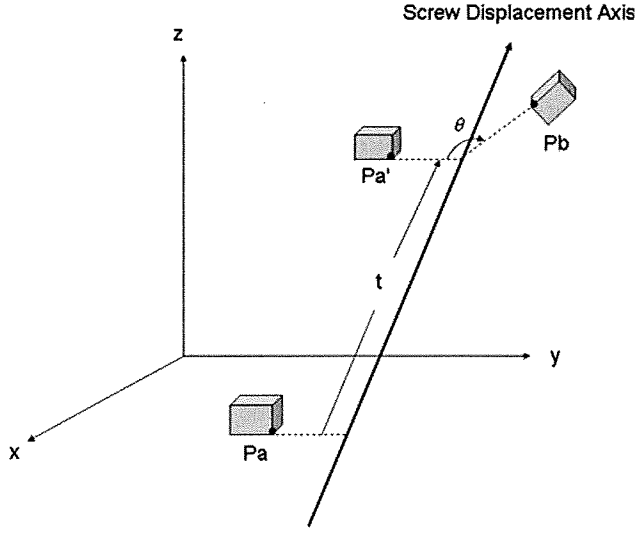

◀ **Fig. 3** General displacement of a rigid body in space can be described by a simultaneous translation along and a rotation about a unique axis. The figure shows the path of the rigid body from *Pa* to *Pb*. First, *Pa* moves to *Pa'* in parallel translation (t) along the unique axis (SDA) and then *Pa* moves to *Pb*, when rotated through $\theta°$ around the axis. Thus, the deformity can be expressed quite simply if one knows the SDA (axis) for the displacement of the distal radius in the current case

Discussion

Premature physeal closure following distal radial fracture in children occurs in about 4–7% of all cases [4, 14, 30] and sometimes results in severe deformity of the wrist [4, 14, 28, 30]. Patients with growth failure of more than 1 cm will have functional problems [4]. Therapeutic options include resection of the physeal bone bridge [12–14], corrective osteotomy [8, 14, 28, 31], epiphysiodesis of the distal ulna

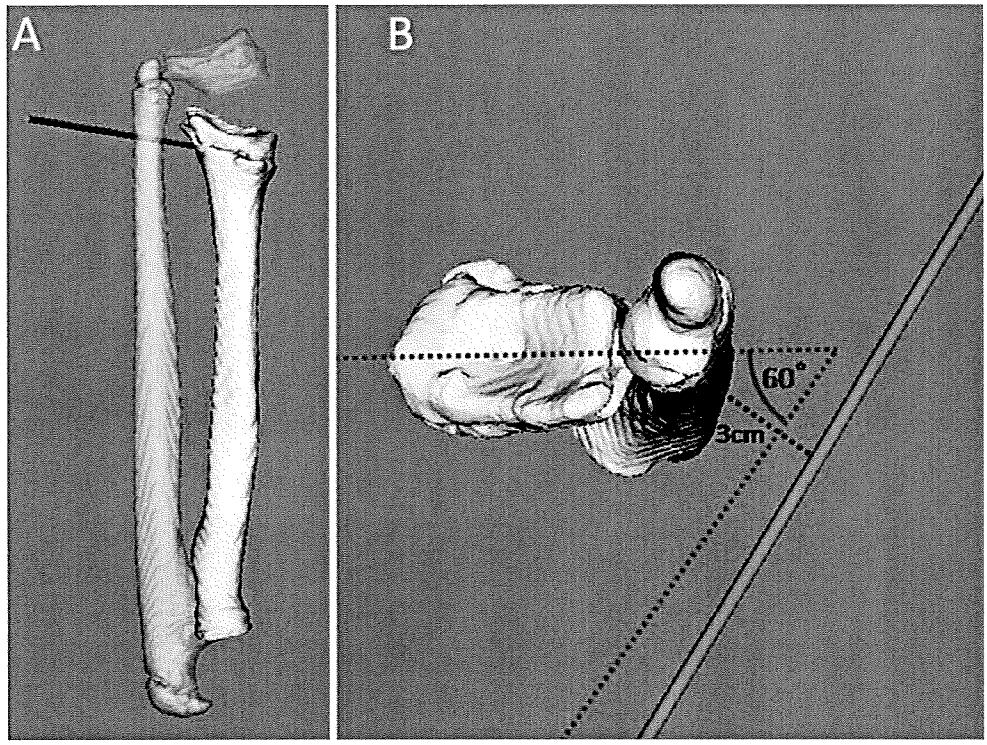

Fig. 4 Simulation results demonstrated that rotation around the axis (*pink*) by 40° brings the distal radius (*solid yellow*) into normal position (*semi-transparent yellow*) (**a**). The axis was 3 cm volar to the wrist joint and had an angle of 60° to the transverse line of the radius (**b**)

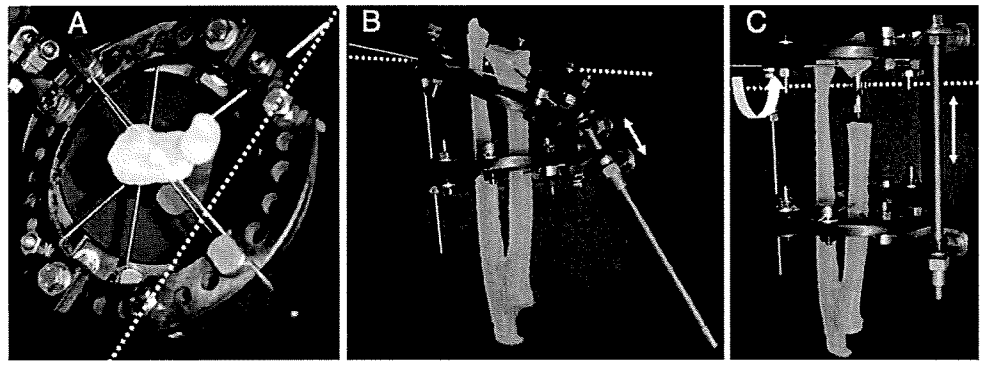

Fig. 5 An Ilizarov external fixator was attached to the full-sized stereolithography bone model. The line connecting the two hinges (*dotted line*) coincided with the simulated axis (**a**). By lengthening only one rod (*arrow*, **b** and **c**), the distal segment was rotated (*curved arrow*, **c**) around the simulated axis. Correction was completed when the two rings became parallel

[28], and radial lengthening [2, 17, 25]. Gradual lengthening and correction with distraction osteogenesis has been indicated for cases with severe deformities [2, 16]. For gradual correction, preoperative planning based on angular correction axis–center of rotation of angulation (ACA–CORA) obtained from radiographic measurements has been widely used [21, 23, 24, 29]. In cases of oblique plane deformity, the axis of deformity and the amount of angulation are calculated using trigonometric functions from measurement results of the anteroposterior, and lateral radiographs [22]. Despite the simplicity of using plain radiographs, accurate calculation of the position of and rotation around the axis of deformity can be difficult, especially in cases of severe periarticular deformity, in which the radiographic contour of the periarticular region is quite different from that of the contralateral normal bone.

With recent advances in CT scanning, however, 3D computer bone models are easily obtained and are becoming widely used in the planning of orthopaedic, and maxillofacial surgery [2, 9, 19, 26]. Use of 3D images to quantify the periarticular deformity enables gradual correction to be planned in a more straightforward and accurate manner. SDA technique, which was employed for the current preoperative simulation, is a method that expresses every body motion in terms of rotation around and translation along a unique axis [11, 27], and has been generally used to iden-

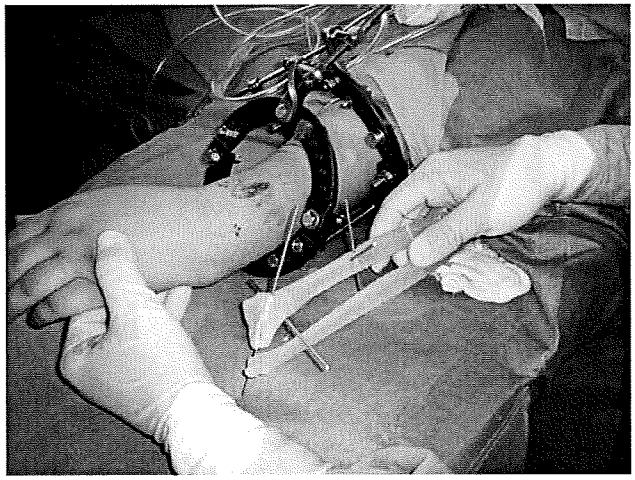

Fig. 6 The external fixator was set up before surgery, and the stereolithography model was sterilized and brought into the operating theater

tify the axis of motion of a joint in biomechanical studies [1, 5]. In several previous studies, the spatial position of the joint axis was calculated using 3D geometrical bone models constructed from CT or MRI data in different joint positions [6, 7, 18]. Consequently, the technique is quite familiar to biomechanical researchers who study joint kinematics. Our findings suggest that the axis of deformity in 3D planning for gradual correction could be determined using the SDA technique, because the deformity is regarded as a motion of the deformed segment relative to the rest of the bone, and we have developed an original computer program that enables us to easily calculate the position of and rotational amount around the axis of deformity by handling 3D bone models [19, 20].

The advantage of our computer simulation approach is its ability to make a very accurate operative plan by calculating the axis of deformity using CT bone models and by presenting it on a 3D viewer. By moving the displaced segment to the normal position with the computer mouse, the operator can have the program instantaneously calculate the 3D axis of deformity and the rotational and translational parameters. The operator can also observe the exact location of the axis from various angles using the 3D viewer. Another advantage of the method is its ability to build real-size mock-ups using the computer data. A stereolithography model is not always necessary for the operation, but in our case we found it useful as a means of confirming the feasibility of the preoperative simulation and to prepare the external fixator properly. The computer program used here

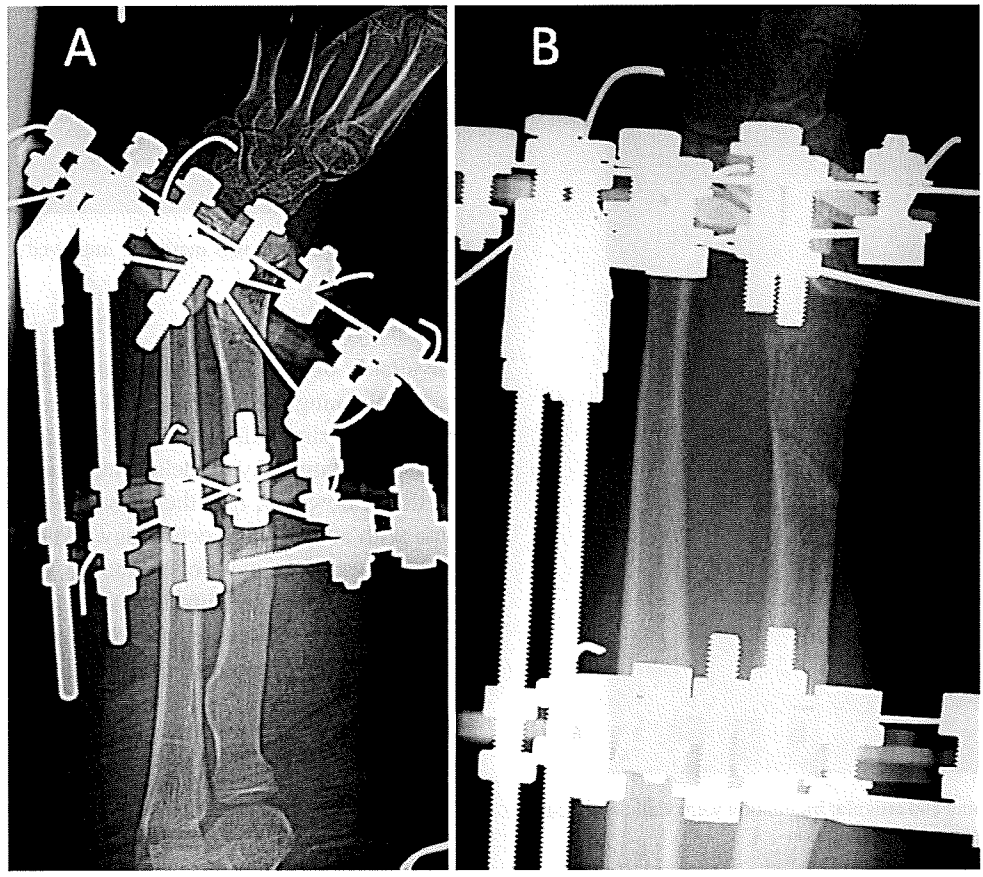

Fig. 7 Lengthening started 1 week after the operation (**a**) and lasted 10 weeks (**b**)

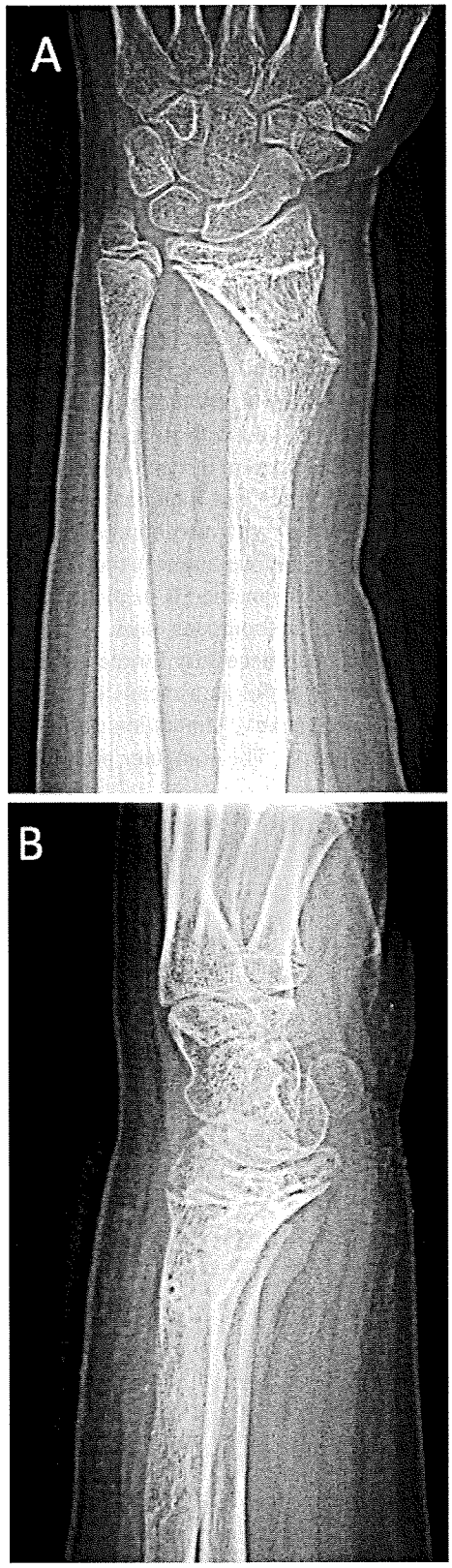

Fig. 8 **a**, **b** Shortening and articular inclination were well corrected, as predicted by the preoperative simulation

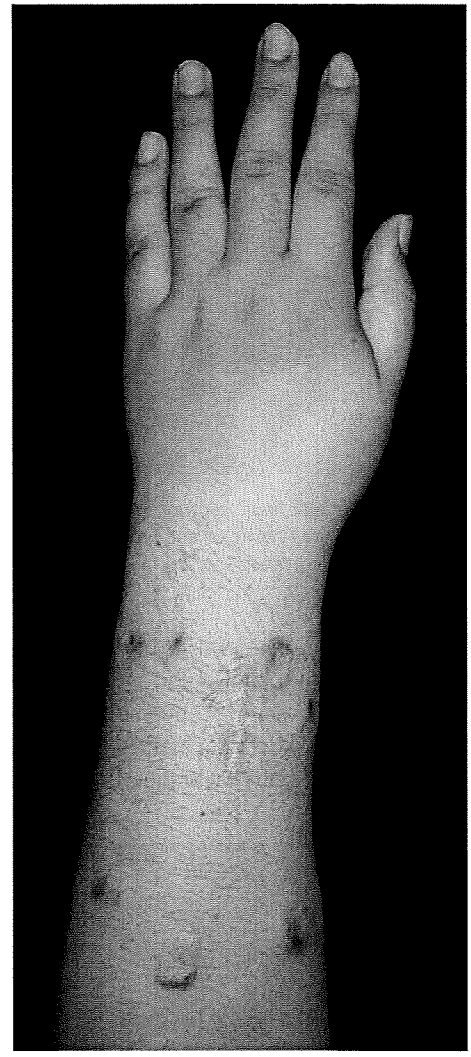

Fig. 9 The appearance was markedly improved after removal of the fixator

is available only in our institution at this stage; however, we are planning to distribute it. The time required for the preoperative simulation was 2 h. The cost of CT scanning and stereolithography modeling may be another drawback. We think, however, that these shortcomings will be overcome with advances in technology and could well be offset by the advantages mentioned above. We believe that our technique of computer simulation is useful in planning corrective surgery for severe limb deformity and hope that it will become the norm in near future to plan such surgeries.

Acknowledgments One of the authors (T.M.) has received a grant from Japan Science and Technology Agency. The authors thank Ryoji Nakao, computer programmer, Department of Orthopaedic Surgery, Osaka University Graduate School of Medicine for his contributions to this study.

References

1. An KN, Chao EY (1984) Kinematic analysis of human movement. Ann Biomed Eng 12:585–597. doi:10.1007/BF02371451
2. Aston JW Jr, Henley MB (1989) Physeal growth arrest of the distal radius treated by the Ilizarov technique. Report of a case. Orthop Rev 18:813–816
3. Athwal GS, Ellis RE, Small CF et al (2003) Computer-assisted distal radius osteotomy. J Hand Surg (Am) 28:951–958. doi:10.1016/S0363-5023(03)00375-7
4. Cannata G, De Maio F, Mancini F et al (2003) Physeal fractures of the distal radius and ulna: long-term prognosis. J Orthop Trauma 17:172–180. doi:10.1097/00005131-200303000-00002
5. Duck TR, Dunning CE, Armstrong AD et al (2003) Application of screw displacement axes to quantify elbow instability. Clin Biomech (Bristol, Avon) 18:303–310. doi:10.1016/S0268-0033(03)00021-4
6. Fischer KJ, Manson TT, Pfaeffle HJ et al (2001) A method for measuring joint kinematics designed for accurate registration of kinematic data to models constructed from CT data. J Biomech 34:377–383. doi:10.1016/S0021-9290(00)00195-0
7. Goto A, Moritomo H, Murase T et al (2004) In vivo elbow biomechanical analysis during flexion: three-dimensional motion analysis using magnetic resonance imaging. J Shoulder Elbow Surg 13:441–447
8. Hove LM, Engesaeter LB (1997) Corrective osteotomies after injuries of the distal radial physis in children. J Hand Surg [Br] 22:699–704. doi:10.1016/S0266-7681(97)80428-7
9. Jupiter JB, Ruder J, Roth DA (1992) Computer-generated bone models in the planning of osteotomy of multidirectional distal radius malunions. J Hand Surg [Am] 17:406–415. doi:10.1016/0363-5023(92)90340-U
10. Kanlic EM, Delarosa F, Pirela-Cruz M (2006) Computer assisted orthopaedic surgery—CAOS. Bosn J Basic Med Sci 6:7–13
11. Kinzel GL, Hall AS Jr, Hillberry BM (1972) Measurement of the total motion between two body segments. I. Analytical development. J Biomech 5:93–105. doi:10.1016/0021-9290(72)90022-X
12. Langenskiold A (1981) Surgical treatment of partial closure of the growth plate. J Pediatr Orthop 1:3–11
13. Langenskiold A, Osterman K (1979) Surgical treatment of partial closure of the epiphysial plate. Reconstr Surg Traumatol 17:48–64
14. Lee BS, Esterhai JL Jr, Das M (1984) Fracture of the distal radial epiphysis. Characteristics and surgical treatment of premature, posttraumatic epiphyseal closure. Clin Orthop Relat Res 185:90–96
15. Lorensen WE, Cline HE (1987) Marching cubes: a high resolution 3D surface construction algorithm. Comput Graph 21:163–169. doi:10.1145/37402.37422
16. Matsubara H, Tsuchiya H, Kabata T et al (2008) Deformity correction for vitamin D-resistant hypophosphatemic rickets of adults. Arch Orthop Trauma Surg 128:1137–1143. doi:10.1007/s00402-007-0548-8
17. Meier R, Prommersberger KJ, van Griensven M et al (2004) Surgical correction of deformities of the distal radius due to fractures in pediatric patients. Arch Orthop Trauma Surg 124:1–9. doi:10.1007/s00402-003-0585-x
18. Moritomo H, Murase T, Goto A et al (2006) In vivo three-dimensional kinematics of the midcarpal joint of the wrist. J Bone Joint Surg Am 88:611–621
19. Murase T, Moritomo H, Goto A et al (2005) Does three-dimensional computer simulation improve results of scaphoid nonunion surgery? Clin Orthop Relat Res 434:143–150
20. Murase T, Oka K, Moritomo H et al (2008) Three-dimensional corrective osteotomy of malunited fractures of the upper extremity with use of a computer simulation system. J Bone Joint Surg Am 90:2375–2389
21. Nakase T, Yasui N, Kawabata H et al (2007) Correction of deformity and shortening due to post traumatic epiphyseal arrest by distraction osteogenesis. Arch Orthop Trauma Surg 127:659–663. doi:10.1007/s00402-007-0339-2
22. Paley D (2002) Oblique plane deformities. In: Paley D (ed) Principles of deformity correction. Springer, Berlin, pp 175–194
23. Paley D, Tetsworth K (1992) Mechanical axis deviation of the lower limbs. Preoperative planning of multiapical frontal plane angular and bowing deformities of the femur and tibia. Clin Orthop Relat Res 280:65–71
24. Rozbruch SR, Paley D, Bhave A et al (2005) Ilizarov hip reconstruction for the late sequelae of infantile hip infection. J Bone Joint Surg Am 87:1007–1018. doi:10.2106/JBJS.C.00713
25. Sabharwal S (2004) Treatment of traumatic radial clubhand deformity with bone loss using the Ilizarov apparatus. Clin Orthop Relat Res 424:143–148. doi:10.1097/01.blo.0000128284.13331.c5
26. Shimizu T, Fujioka F, Gomyo H et al (2003) Three-dimensional starch model for simulation of corrective osteotomy for a complex bone deformity: a case report. Foot Ankle Int 24:364–367
27. Spoor CW, Veldpaus FE (1980) Rigid body motion calculated from spatial co-ordinates of markers. J Biomech 13:391–393. doi:10.1016/0021-9290(80)90020-2
28. Tang CW, Kay RM, Skaggs DL (2002) Growth arrest of the distal radius following a metaphyseal fracture: case report and review of the literature. J Pediatr Orthop B 11:89–92. doi:10.1097/00009957-200201000-00015
29. Waanders NA, Herzenberg JE (1992) The theoretical application of inclined hinges with the Ilizarov external fixator for simultaneous angulation and rotation correction. Bull Hosp Jt Dis 52:27–35
30. Waters PM, Mih AD (2005) Distal radius and ulna fractures. In: Beaty JH, Kasser JR (eds) Fractures in children, 6th edn. Lippincott, Philadelphia, pp 337–398
31. Zehntner MK, Jakob RP, McGanity PL (1990) Growth disturbance of the distal radial epiphysis after trauma: operative treatment by corrective radial osteotomy. J Pediatr Orthop 10:411–415

J Shoulder Elbow Surg (2009) 18, 33-37

ELSEVIER

JOURNAL OF SHOULDER AND ELBOW SURGERY

www.elsevier.com/locate/ymse

Morphologic analysis of the medullary canal in rheumatoid elbows

Akira Goto, MD, PhD[a,*], Tsuyoshi Murase, MD, PhD[a], Jun Hashimoto, MD, PhD[a], Kunihiro Oka, MD, PhD[a], Hideki Yoshikawa, MD, PhD[a], Kazuomi Sugamoto, MD, PhD[b]

[a]*Department of Orthopaedic Surgery, Osaka University Graduate School of Medicine, Suita, Osaka, Japan*
[b]*Department of Orthopaedic Biomaterial Science, Osaka University Graduate School of Medicine, Suita, Osaka, Japan*

Summary Total elbow arthroplasty is a standard approach for patients with arthritic elbows. To design appropriate stems for elbow prostheses, it is important to understand the shape of the medullary canals. The purpose of this study was to evaluate the shape and size of the medullary canals from normal cadavers and rheumatoid arthritis patients. These canals were measured based on geometric constructions of the 3-dimensional bone models generated from computed tomography images. The cross-sectional area of the medullary canals in rheumatoid arthritis patients decreased near the elbow joint as a result of morphologic changes after a long-standing inflammatory reaction. When designing the press-fit component of the humerus, an increase in the width of the transverse diameter of the intramedullary stem could increase stability in the canal. In contrast, for the ulnar component, such morphologic changes would impose difficulty in placing the press-fit model despite an anatomically designed stem. Therefore, a cement technique would be required for improved stabilization of the ulnar component.

Rheumatoid arthritis (RA) is an inflammatory condition, typified by synovial proliferation, that can affect multiple joints, with elbow involvement being the most common in nearly half of RA cases.[12] Total elbow arthroplasty (TEA) in rheumatoid patients is now a widely accepted therapeutic alternative for advanced elbow destruction. The advantage of TEA over simple synovectomy is that it can reduce pain, improve the range of joint motion, and provide long-term pain relief. However, loosening of the implants is one of the major complications and a primary concern. Although the improvement in surgical technique and prosthetic design has led to increased success with TEA, high rates of humeral component loosening have been reported previously.[5,8,18,23,26] Stem design of the prosthesis is considered an important factor that influences loosening of the implant. Data on the geometry of the medullary canals of the distal humerus and proximal ulna should help to design stems for elbow prostheses, which could occupy the medullary cavity, increase its stability with regard to the bone, and decrease the rate of loosening. However, in these patients, it is difficult to evaluate the morphologic analysis appropriately, based only on plain radiographs. In addition, RA patients have shown a restricted range of motion of the elbow with occasional valgus deformity because of erosive changes. Therefore, with only an axial computed tomography (CT) scan, it is difficult to evaluate the morphology accurately. Recent advancements in computer technology have enabled us to determine the precise geometry of the medullary canals generated from the CT data. We have

*Reprint requests: Akira Goto, MD, PhD, Department of Orthopaedic Surgery, Osaka University Graduate School of Medicine, 2-2, Yamada-oka, Suita, Osaka 565-0871, Japan.
E-mail address: goto-akira@umin.ac.jp (A. Goto).

1058-2746/2009/$36.00 - see front matter © 2009 Journal of Shoulder and Elbow Surgery Board of Trustees.
doi:10.1016/j.jse.2008.07.002

constructed 3-dimensional (3D) bone models and resliced the medullary canal vertically along its longitudinal axis to obtain accurate measurements. The purpose of this study was to evaluate the geometry of the medullary canals of the distal humerus and proximal ulna using 3D bone models constructed from the CT data and to compare them between normal cadavers and RA patients.

Materials and methods

We studied the elbow joints of 16 seropositive rheumatoid patients, who were scheduled for TEA (15 women and 1 man; age range, 48-81 years; mean age, 60.6 years) and 20 cadaveric dry bones (10 humeri and 10 ulnae) (Natural Bone; Sawbones [A Division of Pacific Research Laboratories], Vashon, WA). The inclusion criteria for RA patients included RA of grade III to V based on the radiographic criteria of Larsen et al,[10] severe disabling pain, limitation of elbow function, and no previous surgical treatment. Of the patients, 9 (56.2%) had Larsen grade III RA, 4 (25%) had Larsen grade IV RA, and 3 (18.8%) had Larsen grade V RA. The right elbow was affected in 10 patients and the left elbow in 6.

Image acquisition

Morphologic analysis of the medullary canal was performed by use of CT scans. Image data of the elbows from RA patients and cadavers were obtained with a helical CT system (Light Speed Ultra16; GE Medical Systems, Waukesha, WI). We used a sequence with 120 kV, 100 mA, a 300-mm field of view, and a thickness of 0.625 mm on a contiguous slice with a pixel size of 0.39 × 0.39 mm. During CT scanning, the elbow joint was maximally extended with the forearm in a neutral position. Scan data were saved in DICOM (Digital Imaging and Communications in Medicine) format.

Three-dimensional bone models and measurement

Contours and medullary structures of each bone were semiautomatically segmented from CT images by use of the Virtual Place-M software program (Medical Imaging Laboratory, Tokyo, Japan). This software generated 3D surface bone models via the marching cubes technique,[13] based on which we constructed bone models of each humerus and ulna. A threshold for constructing these models is an important parameter for determining their accuracy. In this study, we used 150 Hounsfield units as an optimal threshold value.[21] The contours of the medullary canal were extracted semiautomatically, and the visualization and measurement of the geometric shape and size of each bone were obtained by use of a visualization software program developed in our laboratory. The accuracy of this computer-based measurement was reported to be 0.4 mm.[17]

We resliced the 3D surface bone models of the medullary canal vertically along the longitudinal axis of each canal and evaluated the change in medullary shape of the reconstructed cross section of the humeral medullary canal, from the proximal margin of the olecranon fossa, and for the ulna, from the tip of the coronoid process, at intervals of 1 cm. Then, we calculated the area, as well as the anteroposterior and transverse diameters, of each cross-sectional slice of the medulla of the humerus and the ulna.

Statistical analysis

Mann-Whitney U tests were performed for statistical differences between normal controls and RA patients. A difference with $P < .05$ was considered significant. This statistical analysis was conducted with the Statcel2 statistical analysis software package for personal computers (OMS Publishing, Saitama, Japan).

Results

Morphology of humerus

The cross-sectional shape of the humerus changed from a V shape to an equilateral triangle and then to ovoid in both RA patients and cadavers (Figure 1, *A*). The cross-sectional area particularly decreased at 0 cm above the olecranon fossa compared with the cadavers ($P < .05$). It also tended to decrease at a distance of 1 cm (Figure 2, *A*). Whereas the mean anteroposterior diameter was not significantly different between RA patients and controls, the mean transverse diameter was significantly decreased at 0 and 1 cm in the RA patients as compared with the controls ($P < .05$), as shown in Figures 2, *B*, and 2, *C*. In RA patients and cadavers, the cross-sectional areas were approximately 100 mm^2 at 2 cm and 80 mm^2 at 3 to 10 cm and then they increased gradually at 11 cm. The mean anteroposterior diameters of the humerus tended to increase gradually toward the diaphysis, whereas the transverse diameters gradually decreased.

Morphology of ulna

For the ulna, the shape changed from ovoid to triangular (Figure 1, *B*), and the cross-sectional area decreased at 0 and 1 cm distal to the coronoid process in the RA patients ($P < .05$) (Figure 3, *A*). In the ulna, both the mean anteroposterior and transverse diameters were significantly decreased at 0 and 1 cm, respectively, in the RA patients compared with the controls ($P < .05$) (Figures 3, *B*, and 3, *C*). This discrepancy between RA patients and cadavers was produced by the morphologic changes observed around the trochlear notch of the ulna. In both RA patients and cadavers, the cross-sectional areas were approximately 50 mm^2 at 3 cm and 20 mm^2 at 7 cm to 14 cm. Both the mean anteroposterior and transverse diameters of the ulna tended to decrease gradually toward the diaphysis.

Discussion

TEA can preserve, or even improve, the range of motion of the joints, eliminate pain, and provide adequate stability to the arthritic joint. One major concern regarding TEA is loosening of the implants. Although improvement of surgical technique and prosthetic design has led to

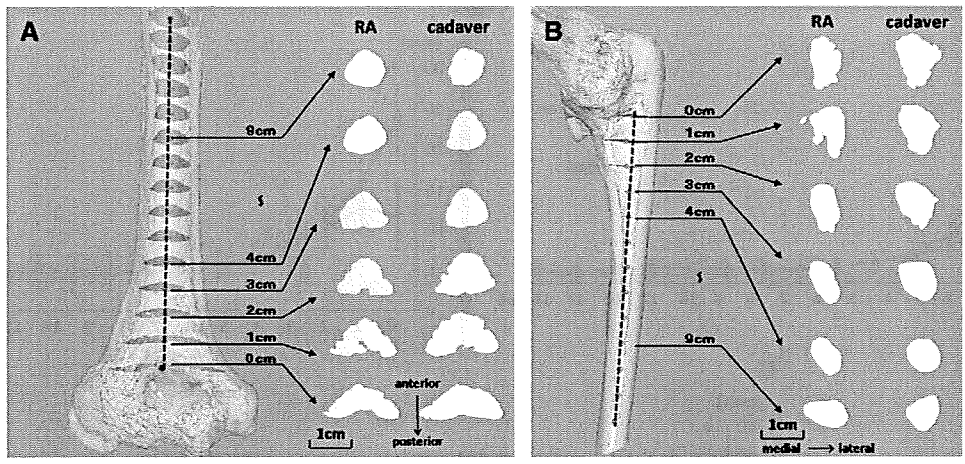

Figure 1 (**A**) Cross-sectional area of medullary canal of humerus. We evaluated the cross-sectional area from the proximal margin of the olecranon fossa at 1-cm intervals. The cross-sectional shape of the humerus changed from a V shape to an equilateral triangle and then to ovoid in both RA patients and cadavers. The cross-sectional area of RA has especially decreased at 0 cm above the olecranon fossa because of the morphologic change around the coronoid fossa, as compared with the cadavers ($P < .05$). (**B**) Cross-sectional area of medullary canal of ulna. The geometric shape of the cross-sectional area changed from ovoid to triangular. In the RA patients, the cross-sectional area decreased at 0 and 1 cm distal to the tip of the coronoid process because of the morphologic change around the trochlear notch of the ulna.

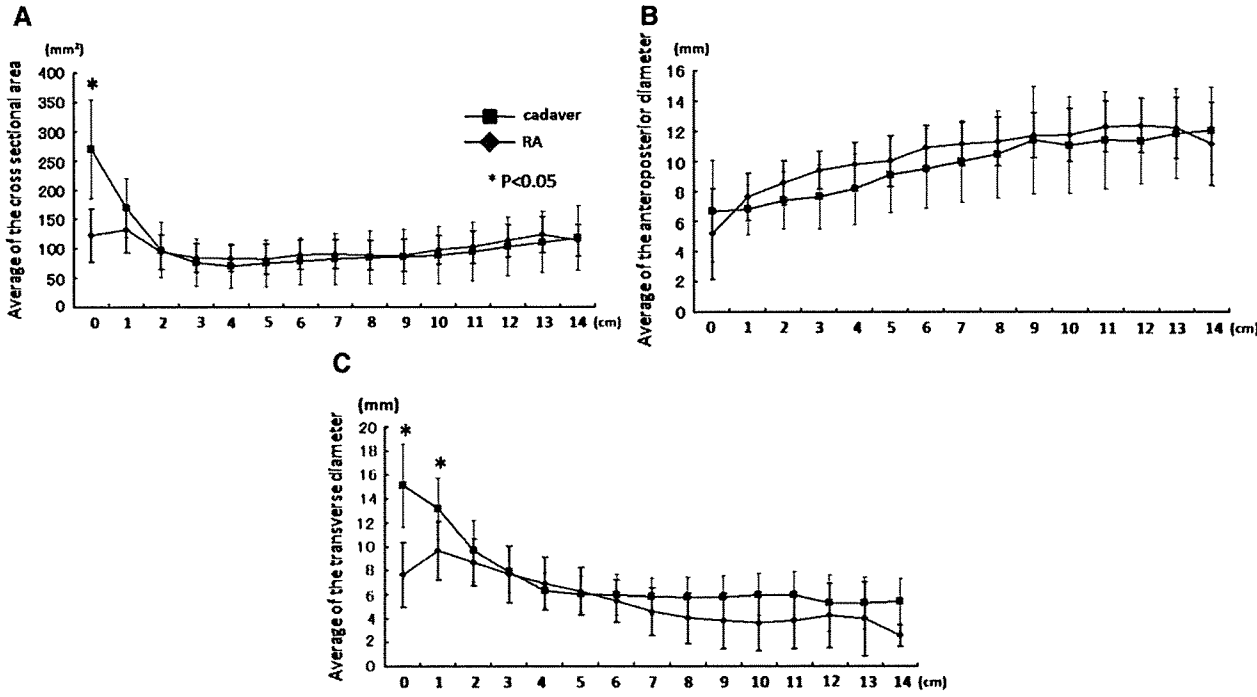

Figure 2 Measurement of medullary canal of humerus. (**A**) The mean cross-sectional area of the humerus is shown with SD error bars. *Asterisk*, A significant difference was found between the RA patients and cadavers ($P < .05$). (**B**) Mean anteroposterior diameters of cross section. (**C**) Mean transverse diameters of cross section.

increased longevity of TEA, the loosening rate is still higher when compared with total hip and knee arthroplasties.[5,6,8,18,19,23,26] In RA patients, van der Lugt et al[26,27] reported that the survival rate of the Souter-Strathclyde prosthesis, according to Kaplan-Meier analysis, was 77.4% after 10 years and 65.2% after 18 years. A high rate of aseptic loosening of the humeral component has been frequently described, whereas the success rate was found to be different among the types of TEA.[5,8,18,23,26] Although several authors postulate that the loosening was because of the micromovement, the reason for this phenomenon remains unclear.[2,24] Ikavalko et al[3,4] reported that the standard stem humeral component has better survivorship compared with the long-stemmed component.

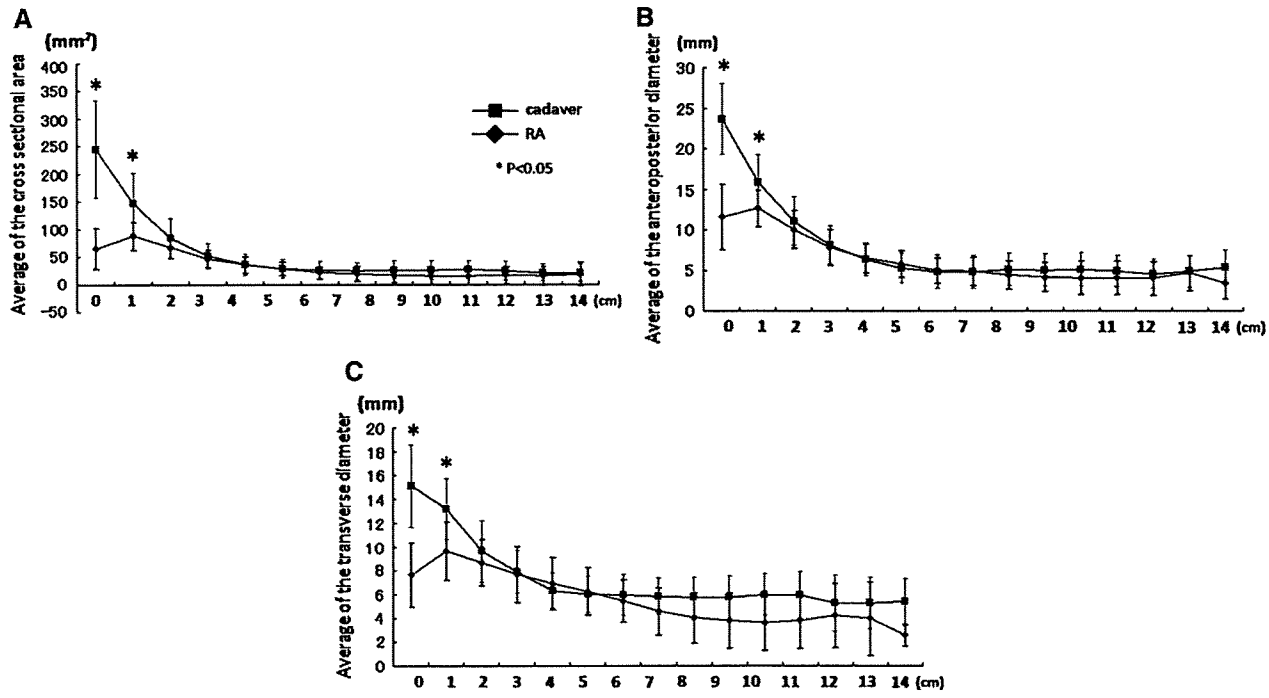

Figure 3 Measurement of medullary canal of ulna. (**A**) The mean cross-sectional area of the ulna is shown with SD error bars. *Asterisk*, A significant difference was found between the RA patients and cadavers ($P < .05$). (**B**) Mean anteroposterior diameters of cross section. (**C**) Mean transverse diameters of cross section.

We assumed that the morphologic change of periarticular inflammatory reaction from arthritis could possibly be one of the reasons for early aseptic loosening after TEA, as it can decrease the stability of the implant in regard to the bone. Therefore, it would be important to evaluate the morphologic change around the elbow joint in RA patients accurately. There have been several detailed studies of the geometry of the medullary canals based on radiographs.[7,11,20] However, it is quite difficult to quantify the extent of the bone loss correctly, based only on plane radiographs.

On the other hand, several authors believe that an anatomic, custom-designed femoral component of total hip arthroplasty is more likely to be effective than off-the-shelf components to achieve the optimal fit and fill the medullary canal.[14,15,28,29] The geometry of the medullary canals of the distal humerus and proximal ulna is considered important for the appropriate design of stems for the TEA prosthesis to increase its stability in the bone and decrease the rate of loosening. Our measurements were derived from 3D constructions of the medullary canal, based on the CT data obtained with a high-speed helical scanner. This allowed us to compare the morphology of the normal controls with the RA group accurately.

High loosening rates of the humeral component have been reported previously.[5,8,18,23,26] On the basis of the data obtained from this study, the anteroposterior diameters of the humerus have tended to increase toward the diaphysis whereas the transverse diameters have decreased (Figure 2, *B*). When considering the initial fixation of the press-fit uncemented stem of the humeral component in future prosthetic design, the width of the transverse diameter is considered more important than the anteroposterior diameter. Increasing the width of the transverse diameter of the intramedullary stem could increase the stability of the humeral component in the canal.

Several authors have noted that aseptic loosening and failure, because of loosening, occur more often with the ulnar component than with the humeral component and that the ulnar component is at high risk of loosening.[1,9,16,22,25] Furthermore, in RA patients, aseptic loosening of the ulnar component was found more often in uncemented ulnar components than in cemented ones. Our results showed that there is a significant morphologic change in the proximal ulnar medullary canal in the area from the coronoid process to 3 cm distally, where the stem of the prosthesis is expected to fit. This change in the morphology would make press fitting of the ulnar component into the canal quite difficult, even with an anatomically designed stem. We believe that the ulnar component would be better stabilized by a cement technique, especially in cases of severe morphologic change.

References

1. Brinkman JM, de Vos MJ, Eygendaal D. Failure mechanisms in uncemented Kudo type 5 elbow prosthesis in patients with rheumatoid arthritis: 7 of 49 ulnar components revised because of loosening after 2-10 years. Acta Orthop 2007;78:263-70.

2. Brunski BJ, Puelo DA, Nanci A. Biomaterials and biomechanics of oral and maxillofacial implants: current state and future developments. Int J Oral Maxillofac Implants 2000;15:15-46.
3. Ikavalko M, Belt EA, Kautiainen H, Lehto MU. Revisions for aseptic loosening in Souter-Strathclyde elbow arthroplasty: incidence of revisions of different components used in 522 consecutive cases. Acta Orthop Scand 2002;73:257-63.
4. Ikavalko M, Lehto MU, Repo A, Kautiainen H, Hamalainen M. The Souter-Strathclyde elbow arthroplasty. A clinical and radiological study of 525 consecutive cases. J Bone Joint Surg Br 2002;84:77-82.
5. Kasten MD, Skinner HB. Total elbow arthroplasty. An 18-year experience. Clin Orthop Relat Res 1993:177-88.
6. Khaw FM, Kirk LM, Gregg PJ. Survival analysis of cemented Press-Fit Condylar total knee arthroplasty. J Arthroplasty 2001;16:161-7.
7. Kitamura T, Hashimoto J, Murase T, Tomita T, Hattori T, Yoshikawa H, et al. Radiographic study of joint destruction patterns in the rheumatoid elbow. Clin Rheumatol 2007;26:515-9.
8. Kraay MJ, Figgie MP, Inglis AE, Wolfe SW, Ranawat CS. Primary semiconstrained total elbow arthroplasty. Survival analysis of 113 consecutive cases. J Bone Joint Surg Br 1994;76:636-40.
9. Landor I, Vavrik P, Jahoda D, Guttler K, Sosna A. Total elbow replacement with the Souter-Strathclyde prosthesis in rheumatoid arthritis. Long-term follow-up. J Bone Joint Surg Br 2006;88:1460-3.
10. Larsen A, Dale K, Eek M. Radiographic evaluation of rheumatoid arthritis and related conditions by standard reference films. Acta Radiol Diagn (Stockh) 1977;18:481-91.
11. Lehtinen JT, Kaarela K, Belt EA, Kauppi MJ, Skyttä E, Kuusela PP, et al. Radiographic joint space in rheumatoid elbow joints. A 15-year prospective follow-up study in 74 patients. Rheumatology (Oxford) 2001;40:1141-5.
12. Lehtinen JT, Kaarela K, Ikävalko M, Kauppi MJ, Belt EA, Kuusela PP, et al. Incidence of elbow involvement in rheumatoid arthritis. A 15 year endpoint study. J Rheumatol 2001;28:70-4.
13. Lorensen WE, Cline HE. Marching cubes: a high resolution 3-D surface construction algorithm. Computer Graphics 1987;21:163-9.
14. McCarthy JC, Bono JV, O'Donnell PJ. Custom and modular components in primary total hip replacement. Clin Orthop Relat Res 1997: 162-71.
15. Mulier JC, Mulier M, Brady LP, Steenhoudt H, Cauwe Y, Goossens M, et al. A new system to produce intraoperatively custom femoral prosthesis from measurements taken during the surgical procedure. Clin Orthop Relat Res 1989:97-112.
16. Potter D, Claydon P, Stanley D. Total elbow replacement using the Kudo prosthesis. Clinical and radiological review with five- to seven-year follow-up. J Bone Joint Surg Br 2003;85:354-7.
17. Robertson DD, Yuan J, Bigliani LU, Flatow EL, Yamaguchi K. Three-dimensional analysis of the proximal part of the humerus: relevance to arthroplasty. J Bone Joint Surg Am 2000;82:1594-602.
18. Rozing P. Souter-Strathclyde total elbow arthroplasty. J Bone Joint Surg Br 2000;82:1129-34.
19. Sathappan SS, Teicher ML, Capeci C, Yoon M, Wasserman BR, Jaffe WL. Clinical outcome of total hip arthroplasty using the normalized and proportionalized femoral stem with a minimum 20-year follow-up. J Arthroplasty 2007;22:356-62.
20. Stein H, Dickson RA, Bentley G. Rheumatoid arthritis of the elbow. Pattern of joint involvement, and results of synovectomy with excision of the radial head. Ann Rheum Dis 1975;34:403-8.
21. Sugano N, Sasama T, Sato Y, Nakajima Y, Nishii T, Yonenobu K, et al. Accuracy evaluation of surface-based registration methods in a computer navigation system for hip surgery performed through a posterolateral approach. Comput Aided Surg 2001;6:195-203.
22. Tanaka N, Kudo H, Iwano K, Sakahashi H, Sato E, Ishii S. Kudo total elbow arthroplasty in patients with rheumatoid arthritis: a long-term follow-up study. J Bone Joint Surg Am 2001;83:1506-13.
23. Trail IA, Nuttall D, Stanley JK. Survivorship and radiological analysis of the standard Souter-Strathclyde total elbow arthroplasty. J Bone Joint Surg Br 1999;81:80-4.
24. Valstar ER, Garling EH, Rozing PM. Micromotion of the Souter-Strathclyde total elbow prosthesis in patients with rheumatoid arthritis 21 elbows followed for 2 years. Acta Orthop Scand 2002; 73:264-72.
25. van der Heide HJ, de Vos MJ, Brinkman JM, Eygendaal D, van den Hoogen FH, de Waal Malefijt MC. Survivorship of the KUDO total elbow prosthesis-comparative study of cemented and uncemented ulnar components: 89 cases followed for an average of 6 years. Acta Orthop 2007;78:258-62.
26. van der Lugt JC, Geskus RB, Rozing PM. Primary Souter-Strathclyde total elbow prosthesis in rheumatoid arthritis. J Bone Joint Surg Am 2004;86:465-73.
27. van der Lugt JC, Rozing PM. Outcome of revision surgery for failed primary Souter-Strathclyde total elbow prosthesis. J Shoulder Elbow Surg 2006;15:208-14.
28. Wettstein M, Mouhsine E, Argenson JN, Rubin PJ, Aubaniac JM, Leyvraz PF. Three-dimensional computed cementless custom femoral stems in young patients: midterm followup. Clin Orthop Relat Res 2005:169-75.
29. Xenakis TA, Gelalis ID, Koukoubis TD, Soucacos PN, Vartziotis K, Kontoyiannis D, et al. Neglected congenital dislocation of the hip: role of computed tomography and computer-aided design for total hip arthroplasty. J Arthroplasty 1996;11:893-8.